nature genetics

ARTICLES

https://doi.org/10.1038/s41588-021-00880-5

Check for updates

Fine-mapping, trans-ancestral and genomic analyses identify causal variants, cells, genes and drug targets for type 1 diabetes

Catherine C. Robertson[1,2,29], Jamie R. J. Inshaw[3,29], Suna Onengut-Gumuscu[1,4], Wei-Min Chen[1,4], David Flores Santa Cruz[3], Hanzhi Yang[1], Antony J. Cutler[3], Daniel J. M. Crouch[3], Emily Farber[1], S. Louis Bridges Jr[5,6], Jeffrey C. Edberg[7], Robert P. Kimberly[7], Jane H. Buckner[8], Panos Deloukas[9,10], Jasmin Divers[11], Dana Dabelea[12], Jean M. Lawrence[13], Santica Marcovina[14,28], Amy S. Shah[15], Carla J. Greenbaum[16,17], Mark A. Atkinson[18], Peter K. Gregersen[19], Jorge R. Oksenberg[20], Flemming Pociot[21,22,23], Marian J. Rewers[24], Andrea K. Steck[24], David B. Dunger[25,26], Type 1 Diabetes Genetics Consortium*, Linda S. Wicker[3], Patrick Concannon[18,27], John A. Todd[3,30] ✉ and Stephen S. Rich[1,4,30]

We report the largest and most diverse genetic study of type 1 diabetes (T1D) to date (61,427 participants), yielding 78 genome-wide-significant ($P < 5 \times 10^{-8}$) regions, including 36 that are new. We define credible sets of T1D-associated variants and show that they are enriched in immune-cell accessible chromatin, particularly CD4$^+$ effector T cells. Using chromatin-accessibility profiling of CD4$^+$ T cells from 115 individuals, we map chromatin-accessibility quantitative trait loci and identify five regions where T1D risk variants co-localize with chromatin-accessibility quantitative trait loci. We highlight rs72928038 in *BACH2* as a candidate causal T1D variant leading to decreased enhancer accessibility and *BACH2* expression in T cells. Finally, we prioritize potential drug targets by integrating genetic evidence, functional genomic maps and immune protein–protein interactions, identifying 12 genes implicated in T1D that have been targeted in clinical trials for autoimmune diseases. These findings provide an expanded genomic landscape for T1D.

Type 1 diabetes (T1D) is characterized by an autoimmune attack on insulin-producing β-cells in the pancreatic islets, driven by diverse genetic[1–6] and environmental[7] factors. Genetic screening and autoantibody surveillance can detect islet autoimmunity before overt progression to T1D[8–10], providing an opportunity for prevention. Multiple immune therapies have been explored in clinical trials[11]. A 14-day course of teplizumab, an anti-CD3 monoclonal antibody, was recently demonstrated to delay T1D in individuals

[1]Center for Public Health Genomics, University of Virginia, Charlottesville, VA, USA. [2]Department of Biochemistry and Molecular Genetics, University of Virginia, Charlottesville, VA, USA. [3]JDRF/Wellcome Diabetes and Inflammation Laboratory, Wellcome Centre for Human Genetics, Nuffield Department of Medicine, NIHR Oxford Biomedical Research Centre, University of Oxford, Oxford, UK. [4]Department of Public Health Sciences, University of Virginia, Charlottesville, VA, USA. [5]Division of Rheumatology, Department of Medicine, Hospital for Special Surgery, New York, NY, USA. [6]Division of Rheumatology, Department of Medicine, Weill Cornell Medical College, New York, NY, USA. [7]Division of Clinical Immunology and Rheumatology, Department of Medicine, University of Alabama at Birmingham, Birmingham, AL, USA. [8]Center for Translational Immunology, Benaroya Research Institute, Seattle, WA, USA. [9]Clinical Pharmacology, William Harvey Research Institute, Barts and the London School of Medicine and Dentistry, Queen Mary University of London, London, UK. [10]Princess Al-Jawhara Al-Brahim Centre of Excellence in Research of Hereditary Disorders (PACER-HD), King Abdulaziz University, Jeddah, Saudi Arabia. [11]Division of Health Services Research, Department of Foundations of Medicine, New York University Long Island School of Medicine, Mineola, NY, USA. [12]Colorado School of Public Health and Lifecourse Epidemiology of Adiposity and Diabetes (LEAD) Center, University of Colorado Anschutz Medical Campus, Aurora, CO, USA. [13]Department of Research and Evaluation, Kaiser Permanente Southern California, Pasadena, CA, USA. [14]Northwest Lipid Metabolism and Diabetes Research Laboratories, University of Washington, Seattle, WA, USA. [15]Cincinnati Children's Hospital Medical Center and the University of Cincinnati, Cincinnati, OH, USA. [16]Center for Interventional Immunology, Benaroya Research Institute, Seattle, WA, USA. [17]Diabetes Program, Benaroya Research Institute, Seattle, WA, USA. [18]Department of Pathology, Immunology, and Laboratory Medicine, University of Florida, Gainesville, FL, USA. [19]Robert S. Boas Center for Genomics and Human Genetics, Feinstein Institutes for Medical Research, Northwell Health, Manhasset, NY, USA. [20]Department of Neurology and Weill Institute for Neurosciences, University of California at San Francisco, San Francisco, CA, USA. [21]Department of Pediatrics, Herlev University Hospital, Copenhagen, Denmark. [22]Institute of Clinical Medicine, Faculty of Health and Medical Sciences, University of Copenhagen, Copenhagen, Denmark. [23]Type 1 Diabetes Biology, Department of Clinical Research, Steno Diabetes Center Copenhagen, Gentofte, Denmark. [24]Barbara Davis Center for Diabetes, School of Medicine, University of Colorado Anschutz Medical Campus, Aurora, CO, USA. [25]Department of Paediatrics, University of Cambridge, Cambridge, UK. [26]Wellcome Trust Medical Research Council Institute of Metabolic Science, University of Cambridge, Cambridge, UK. [27]Genetics Institute, University of Florida, Gainesville, FL, USA. [28]Present address: Medpace Reference Laboratories, Cincinnati, OH, USA. [29]These authors contributed equally: Catherine C. Robertson, Jamie R. J. Inshaw. [30]These authors jointly supervised this work: John A. Todd, Stephen S. Rich. *A list of authors and their affiliations appears at the end of the paper. ✉e-mail: jatodd@well.ox.ac.uk

with a high genetic risk for T1D by a median of two years[12]. This success shows that appropriately timed immune-modulating therapy can alter the autoimmune process preceding disease onset. Defining the genetic variants contributing to T1D risk and how they disrupt immune pathways may lead to more precise therapeutic targets, better characterization of their role in disease initiation and progression, and improved opportunities for safe and effective intervention and, ultimately, prevention of T1D[13,14].

Approximately 60 genomic regions have been associated with T1D risk in individuals of European (EUR) ancestry[1–3,15–21]. However, less is known for individuals of non-EUR ancestry, despite recent increases in T1D diagnoses in these understudied populations[22]. In addition, the mechanisms underlying most T1D associations are unknown. We showed previously that T1D credible variants are most strongly enriched in lymphocyte and thymic enhancers[3]. However, resolving causal variants, mapping them to genes and determining the causal mechanisms remains a challenge.

Here we double the sample size from the previous largest T1D study, genotype ancestrally diverse T1D cases, controls and affected families, and impute additional variants[23]. Using this expanded dataset, we perform discovery and fine-mapping analyses. In T1D-associated regions, we use chromatin-accessibility quantitative trait loci (caQTL) to prioritize credible variants for interrogation of the molecular mechanisms underlying T1D association. We present a compelling hypothesis of a genetic regulatory mechanism in the T1D locus encoding the transcription factor BACH2. Finally, by integrating the implicated genes with immune protein networks, we identify drugs that target T1D candidate genes and networks.

Results

Thirty-six new genome-wide-significant regions. After quality filtering (Supplementary Fig. 1 and Methods), 61,427 participants (Supplementary Table 1) and 140,333 genotyped ImmunoChip variants were included in our analyses, providing dense coverage in 188 autosomal regions ('ImmunoChip regions')[24] and sparse genotyping in other regions (Supplementary Tables 2 and 3). Each participant was assigned to one of five ancestry groups by using principal-component analysis (Methods and Supplementary Fig. 2): EUR ($n=47{,}319$), African admixed (AFR, $n=4{,}290$), Finnish (FIN, $n=6{,}991$), East Asian (EAS, $n=588$) and Other admixed (AMR, $n=2{,}239$). The association analyses included 16,159 T1D cases, 25,386 controls and 6,143 trio families (that is, an affected child and both parents; Supplementary Tables 4,5 and Supplementary Fig. 3). Genotypes at additional variants were imputed using the Trans-Omics for Precision Medicine (TOPMed)[23] multi-ancestry reference panel to improve discovery and fine-mapping resolution (Methods). After imputation, the number of variants in ImmunoChip regions with a Minimac4 estimated imputation accuracy (r^2) > 0.8 and minor allele frequency (MAF) > 0.005 in each ancestry group was 166,274 (EUR), 322,084 (AFR), 163,612 (FIN), 137,730 (EAS) and 188,550 (AMR). We compared the imputed genotypes with whole-genome sequencing data from a subset of individuals and observed high concordance (Methods, Supplementary Note and Supplementary Figs. 4,5).

Initially, we analyzed unrelated cases and controls ($n=41{,}545$), assuming an additive inheritance model. With minimal evidence of artificial inflation of association statistics due to population structure (Supplementary Note, Supplementary Fig. 6 and Supplementary Table 6), we identified 64 T1D-associated regions outside the major histocompatibility complex (MHC; including the human-leukocyte-antigen loci), including 24 new regions associated with T1D at genome-wide significance ($P<5\times10^{-8}$). Following conditional analysis, 78 independent associations were identified ($P<5\times10^{-8}$; Supplementary Table 7). On the X chromosome, the most T1D-associated variant was rs4326559 (A>C; C-allele odds ratio (OR) = 1.09, $P=4.5\times10^{-7}$).

We extended the discovery analysis to incorporate T1D trio families ($n=6{,}143$ trios, some trio families were multiplex and analyzed as multiple trios; Methods). A meta-analysis of the case-control and trio results identified 78 chromosome regions associated with T1D ($P<5\times10^{-8}$), including 42/43 chromosome regions previously identified in an ImmunoChip-based study[3] (rs4849135 (G>T) with $P=2.93\times10^{-7}$). When we compared these 78 regions with previous T1D studies[1–3,15–21], 36 new regions were found to be associated with T1D at genome-wide significance (Table 1). In the remaining 42 regions, the lead variant was within 250 kb of the lead variant in a previous T1D study. The 1q21.3 region, which contains the gene encoding the interleukin-6 receptor (IL-6R), was among the newly identified regions associated with T1D at genome-wide significance. Interestingly, the lead variant in this region was rs2229238 (NC_000001.11:g.154465420T>C; $P=3.02\times10^{-9}$), not the nonsynonymous variant rs2228145 (NC_000001.11:g.154454494A>C, NP_000556.1:p.Asp358Ala; $P=2.20\times10^{-4}$), which was previously suggested to be causal for T1D in targeted analysis[25] and remains a candidate causal variant for rheumatoid arthritis[26].

Additional regions identified using alternative inheritance models and metric of statistical significance. With the Benjamini–Yekutieli false discovery rate (FDR) < 0.01 (ref. [27]) to assess statistical significance, 143 regions were found to be associated with T1D (Supplementary Table 8). Their lead variants overlapped substantially with the lead variants for 14 immune-mediated diseases from published studies, but the direction of effects frequently differed between traits (Supplementary Fig. 7). Compared with variants satisfying genome-wide significance, associated variants with an FDR < 0.01 that did not meet genome-wide significance ($P<5\times10^{-8}$) had smaller absolute effect sizes (median OR = 1.07 (interquartile range 1.06–1.09) versus median OR = 1.11 (interquartile range 1.09–1.13)) but similar MAFs (median MAF = 0.301 (interquartile range 0.152–0.397) versus median MAF = 0.306 (interquartile range 0.184–0.374)). These results indicate that the remaining regions associated with T1D may have increasingly smaller effect sizes (Supplementary Fig. 8), requiring genome-wide coverage and larger sample sizes for detection.

One exception underscores the need for the inclusion of understudied populations to enhance biological insight, even with limited sample sizes, and suggests the potential value of considering alternative metrics for defining statistical significance in genetic studies[28]. On chromosome 1p22.1, near the metal response element binding transcription factor 2 (*MTF2*) gene, rs190514104 (NC_000001.11:g.93145882G>A) had a large effect on T1D risk (OR (95% confidence interval) = 2.9 (1.9–4.5); $P=6.6\times10^{-7}$) in the AFR ancestry group. The minor allele (A) at rs190514104:G>A was common in the AFR ancestry group (>1%) but rare in the others (<0.1%). Considering the limited sample size, potential heterogeneity of the AFR cohort and possible overestimation of effect sizes due to 'the winner's curse', this association requires replication in an independent cohort.

Through the use of recessive and dominant models of inheritance, 35 regions (25 dominant and 10 recessive) with a better fit than the additive model were identified (lower Akaike information criterion (AIC) in the EUR group) at FDR < 0.01, including nine regions that did not reach FDR < 0.01 under the additive model (Supplementary Table 9). Thus, a total of 152 regions were associated with T1D at FDR < 0.01, 143 under an additive model and nine under recessive or dominant models.

Fine mapping revealed that over a third of the T1D loci contain more than one independent association. To define the local architecture of the T1D regions, we applied a Bayesian stochastic search method (GUESSFM[29]) to the EUR-ancestry case-control data ('Statistical fine mapping' section in Methods). Of 52 ImmunoChip regions (Supplementary Table 2) associated with T1D, GUESSFM

Table 1 | Newly identified regions of association with T1D with genome-wide significance ($P < 5 \times 10^{-8}$)

Chromosome	Position (bp)[a]	Lead variant rsID	A1	A2	Putative candidate gene[b]	AF_{EUR} (A2)	OR_{meta}[c]	P_{meta}	Traits with shared association[d]
1	63643100	rs2269241	T	C	*PGM1*	0.196	1.111	4.67×10^{-12}	
1	92358141	rs34090353	G	C	*RPAP2*	0.361	1.078	1.10×10^{-8}	
1	119895261	rs2641348	A	G	*NOTCH2*	0.107	1.113	1.61×10^{-8}	Crohn's disease, T2D
1	154465420	rs2229238	T	C	*IL6R*	0.813	0.896	1.38×10^{-12}	
1	172746562	rs78037977	A	G	*FASLG*	0.124	0.884	2.41×10^{-9}	Asthma, vitiligo, allergic sensitization
1	192570207	rs2816313	G	A	*RGS1*	0.719	1.090	4.57×10^{-9}	
1	212796238	rs11120029	G	T	*TATDN3*	0.147	1.102	1.82×10^{-8}	
2	12512805	rs10169963	C	T	AC096559.1	0.580	1.074	2.78×10^{-8}	
2	100147438	rs12712067	G	T	*AFF3*	0.358	0.925	4.12×10^{-9}	
2	191105394	rs7582694	C	G	*STAT4*	0.773	0.916	2.83×10^{-9}	SLE, hypothyroidism, celiac disease, RA
2	241468331	rs10933559	A	G	*FARP2*	0.208	1.109	2.39×10^{-11}	
4	973543	rs113881148	C	A	*TMEM175*	0.626	1.082	5.72×10^{-9}	Body-fat percentage
4	38602849	rs337637	G	A	*KLF3*	0.364	0.919	2.57×10^{-10}	White blood-cell count
5	40521603	rs1876142	G	T	*PTGER4*	0.658	0.905	2.18×10^{-14}	
5	56146422	rs10213692	T	C	*ANKRD55/IL6ST*	0.241	0.912	2.85×10^{-9}	RA, Crohn's disease, MS
6	424915	rs9405661	C	A	*IRF4*	0.514	1.080	2.26×10^{-9}	
6	137682468	rs12665429	T	C	*TNFAIP3*	0.370	0.907	1.36×10^{-13}	
6	159049210	rs212408	G	T	*TAGAP*	0.638	1.112	1.42×10^{-15}	MS, Crohn's disease, eczema
7	20557306	rs17143056	A	G	*ABCB5*	0.183	0.909	2.44×10^{-8}	
7	28102567	rs10245867	G	T	*JAZF1*	0.331	0.928	3.15×10^{-8}	Eczema, hay fever, MS, SLE, monocyte percentage
8	11877675	rs2250903	G	T	*CTSB*	0.283	0.905	1.35×10^{-10}	
9	99823263	rs1405209	T	C	*NR4A3*	0.375	1.075	3.45×10^{-8}	
10	33137219	rs722988	T	C	*NRP1*	0.367	1.108	3.21×10^{-15}	
11	35267496	rs11033048	C	T	*SLC1A2*	0.366	1.091	1.53×10^{-10}	Vitiligo
11	60961822	rs79538630	G	T	*CD5/CD6*	0.035	1.213	1.14×10^{-9}	
11	61828092	rs968567	C	T	*FADS2*	0.177	0.903	8.42×10^{-9}	RA, neutrophil percentage
11	64367826	rs645078	A	C	*CCDC88B*	0.385	0.925	3.34×10^{-9}	
11	128734337	rs605093	G	T	*FLI1*	0.470	1.077	4.25×10^{-9}	
12	8942630	rs1805731	T	C	*M6PR*	0.389	1.073	4.16×10^{-8}	Eosinophil count
12	53077434	rs7313065	C	A	*ITGB7*	0.162	1.101	3.28×10^{-9}	
13	42343795	rs74537115	C	T	*AKAP11*	0.141	1.109	5.41×10^{-9}	
14	68286876	rs911263	C	T	*RAD51B*	0.710	1.083	1.69×10^{-8}	PBC, SLE, RA
16	20331769	rs4238595	T	C	*UMOD*	0.687	0.912	2.43×10^{-11}	
17	45996523	rs1052553	A	G	*MAPT*	0.232	0.879	1.65×10^{-15}	Parkinson's disease
17	47956725	rs2597169	A	G	*PRR15L*	0.348	1.081	3.35×10^{-9}	
21	44204668	rs56178904	C	T	*ICOSLG*	0.187	0.898	6.48×10^{-11}	

Of these 36 regions, 13 had a lead variant that was in strong linkage disequilibrium ($r^2 > 0.95$ in the 1000 Genomes Project European population) with variants that are associated with at least one related trait. [a]Genome build 38. [b]Closest gene or gene with mechanistic support from the literature. [c]Additive OR for the addition of an A2 allele. [d]Related traits (https://genetics.opentargets.org) where the lead variant is in strong LD ($r^2 > 0.95$ in the 1000 Genomes Project European population) with T1D lead variant. RA, rheumatoid arthritis; T2D, type 2 diabetes; SLE, systemic lupus erythematosus; MS, multiple sclerosis; IBD, inflammatory bowel disease; PBC, primary biliary cholangitis.

predicted 21 (40%) to contain more than one causal variant (Fig. 1a), compared with nine regions using stepwise conditional regression. The lead variant in the discovery analysis was not prioritized by fine mapping (posterior probability < 0.5) in four regions: 2q33.2 (*CTLA4*), 4q27 (*IL2*), 14q32.2 (*MEG3*) and 21q22.3 (*UBASH3A*). In these regions, the lead variant is likely to tag two or more T1D-associated haplotypes that can be identified using GUESSFM but not stepwise logistic regression, a phenomenon that has been observed previously[29,30]. For example, although stepwise regression analysis in the *UBASH3A* locus provided support for a single causal variant (Supplementary Table 7), GUESSFM fine mapping and haplotype analyses indicated that the lead variant in this region, rs11203203 (NC_000021.9:g.42416077G>A), is unlikely to be causal. GUESSFM fine mapping supported a three-variant model

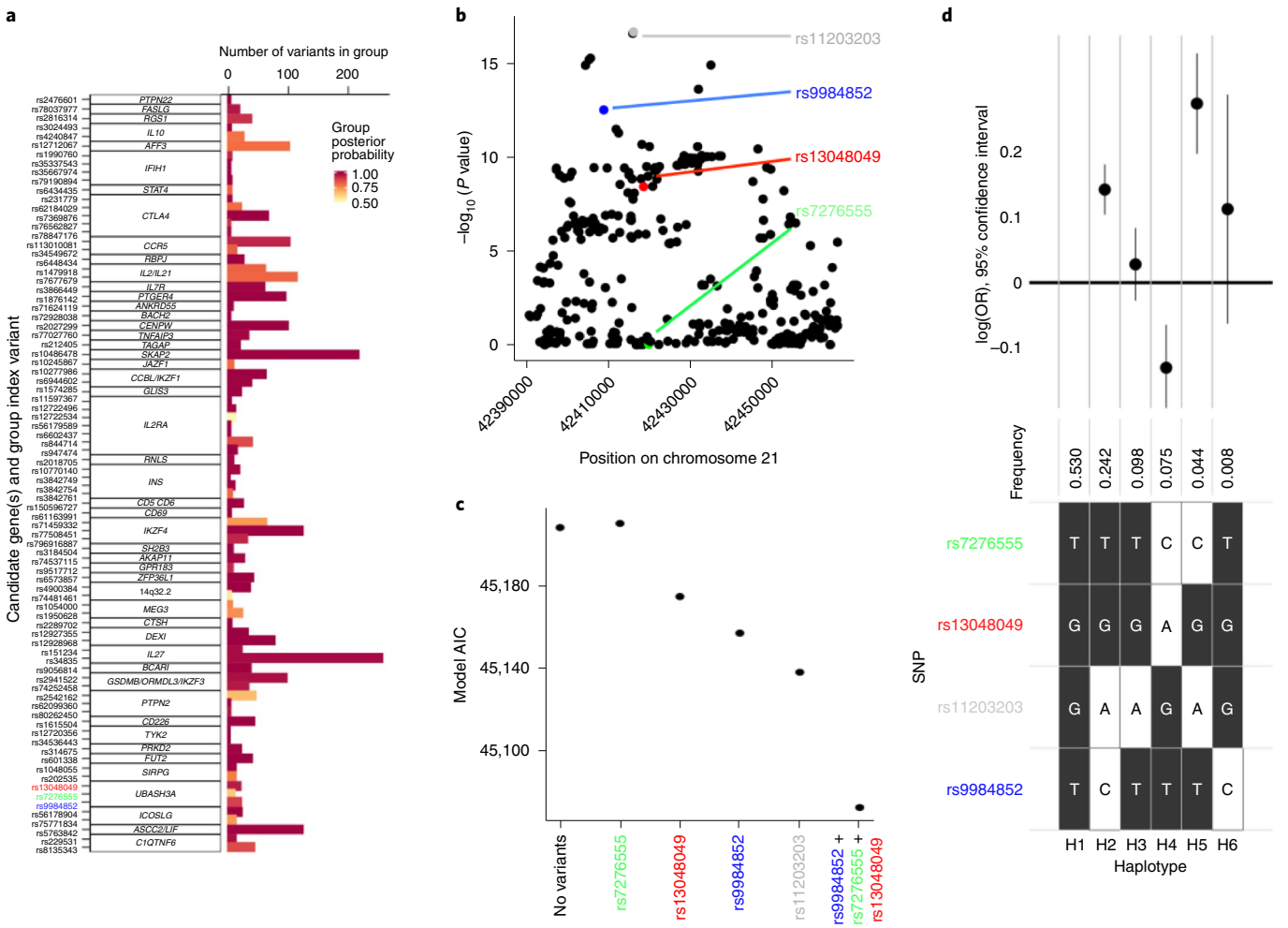

Fig. 1 | Fine mapping of T1D regions using a Bayesian stochastic search algorithm. a, Number of variants in GUESSFM-prioritized groups with group posterior probability > 0.5. The candidate gene names and lead variants for each group are shown on the *y* axis. **b**, Manhattan plot of the *UBASH3A* region from the EUR case-control analysis highlighting the lead variant from the univariable analysis rs11203203:G>A (gray) and the three variants prioritized using GUESSFM—rs9984852:T>C (blue), rs13048049:G>A (red) and rs7276555:T>C (green). **c**, Comparison of model AIC in the *UBASH3A* region for models fit using EUR cases and controls only, comparing combinations of alleles prioritized either in univariable (gray) or GUESSFM analyses (red, green and blue). **d**, Analysis of haplotypes associated with T1D in the *UBASH3A* region. The most common haplotype (H1: T-G-G-T for rs7276555-rs13048049-rs11203203-rs9984852) is presented on the far left; alternative haplotypes (H2–H6) are shown with white squares highlighting the differentiating alleles (C, A, A or C, respectively). The frequency and effect estimates for association with T1D relative to the baseline haplotype (H1) are shown above the grid (the point and error bars represent the log-transformed OR and 95% confidence interval of the log-transformed OR, respectively); for example, the log-transformed OR for T1D risk for haplotype H3 (T-G-A-T) relative to the baseline haplotype (H1) is close to zero and the 95% confidence interval crosses zero. Haplotype analyses were performed based on $n = 33{,}601$ unrelated EUR individuals (13,458 T1D cases and 20,143 controls).

(rs9984852 (NC_000021.9:g.42408836T>C), rs13048049 (NC_000021.9:g.42418534G>A) and rs7276555 (NC_000021.9:g.42419803T>C); Fig. 1b), which had a better fit than the single variant model (AIC 45,073 versus 45,138; Fig. 1c). Haplotype analysis (Methods) demonstrated that when rs11203203:G>A is present without the GUESSFM-prioritized variants, there is no effect of rs11203203:G>A on T1D risk (Fig. 1d). Resampling experiments consistently supported two or more causal variants in the region, with at least one of the three GUESSFM-prioritized variants more likely to be causal than rs11203203:G>A (Supplementary Table 10). Given the complexity of association in the *UBASH3A* region, and probably at many loci, statistical methods designed to use univariable summary statistics alone are not sufficient to explore the genetic architecture of T1D. We have provided the comprehensive list of T1D credible variants and haplotype analyses for all 52 fine-mapped regions (Supplementary Table 11, https://github.com/ccrobertson/t1d-immunochip-2020).

Differences in linkage disequilibrium (LD) between ancestry groups can be advantageous in prioritizing causal variants[31]. We performed multi-ancestry fine mapping using PAINTOR[32] for the 30 regions where analyses suggested a single causal variant. For eight regions, an associated variant ($P < 5 \times 10^{-4}$) was identified in more than one ancestry group: five with associations in EUR and FIN, and three with associations in EUR and AFR. In three regions, the number of variants prioritized was markedly reduced by including multiple ancestry groups (Supplementary Table 12): 4p15.2 (*RBPJ*; Fig. 2), 6q22.32 (*CENPW*; Extended Data Fig. 1) and 18q22.2 (*CD226*; Extended Data Fig. 2). In the chromosome 4p15.2 (*RBPJ*) region, the credible set from EUR ancestry contained 24 variants. In contrast, using PAINTOR with EUR and AFR summary statistics, only five variants were prioritized with a posterior probability > 0.1 (Fig. 2a). Among these prioritized variants, rs34185821 (NC_000004.12:g.26083858A>G) and rs35944082 (NC_000004.12:g.26093692A>G), both located in the noncoding transcript *LINC02357*,

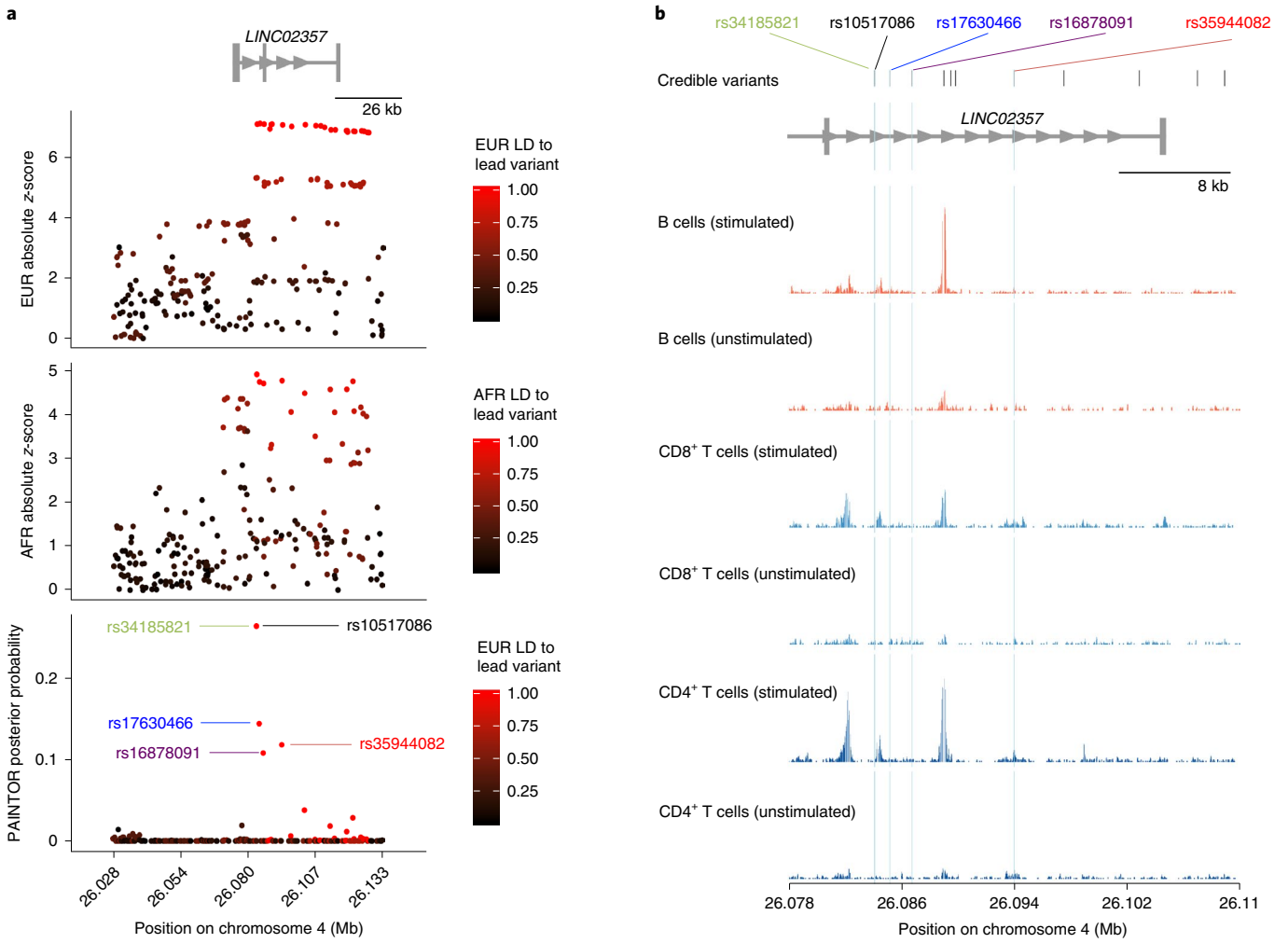

Fig. 2 | Fine mapping of the chromosome 4p15.2 region. a, Association *z*-score statistics for the EUR (top) and AFR (middle) ancestry groups; posterior probabilities (bottom) from multi-ancestry fine mapping of the EUR and AFR groups using PAINTOR. The *z*-scores are colored according to the LD value to the lead PAINTOR-prioritized variant. **b**, Overlay of T1D credible variants with open chromatin ATAC-seq peaks in immune cells, with the variants prioritized by PAINTOR (posterior probability > 0.1) indicated with blue dashed lines. The normalized ATAC-seq read count is shown for stimulated and unstimulated CD4+ T cells, CD8+ T cells and B cells.

have the potential to disrupt multiple transcription-factor binding motifs[33]. The rs35944082:A>G variant also overlaps open chromatin in multiple adaptive immune-cell types (Fig. 2b) and resides in a FANTOM enhancer site[34]. Furthermore, rs34185821:A>G is one of three prioritized variants flanking an activation-dependent assay for transposase-accessible chromatin using sequencing (ATAC-seq) peak in lymphocytes and a stable response element in human islets[35], with potential to perturb an extended TATA-box motif[36].

T1D-associated protein-altering variants. Only 34/2,732 (1.2%) credible variants (group posterior probability > 0.5) were protein-altering (nonsynonymous, frameshift, stop-gain or splice-altering) with 12 providing support for a role in T1D (Methods and Supplementary Table 13). We identified several previously unreported protein-altering variants as highly prioritized in the T1D credible sets (posterior probability > 0.1): a protective missense variant in *UBASH3A* (rs13048049:G>A, NP_061834.1:p.Arg324Gln; OR = 0.84 and EUR allele frequency (AF_{EUR}) = 0.051), two low-frequency splice donor variants in *IFIH1* (rs35732034, NC_000002.12:g.162268086C>T; OR = 0.63 and AF_{EUR} = 0.0089; and rs35337543, NC_000002.12:g.162279995C>G; OR = 0.61 and AF_{EUR} = 0.0099) and a missense variant in *CTLA4* (rs231775, NC_000002.12:g.203867991A>G, NP_001032720.1:p.Thr17Ala; OR = 1.20 and AF_{EUR} = 0.36).

T1D credible variants are overrepresented in the accessible chromatin of T and B cells. ATAC-seq offers a high-resolution map of accessible chromatin with potential regulatory function[37]. Using publicly available[38–40] and newly generated ATAC-seq data from healthy donors, we assessed the enrichment (Methods) of 2,431 T1D credible variants (group posterior probability > 0.8) in accessible chromatin across diverse immune and non-immune-cell types (including 25 primary immune-cell types, pancreatic islets and, as control cell types unlikely to be central to T1D etiology, fetal and adult cardiac fibroblasts). T1D credible variants were enriched in the open chromatin of multiple primary immune-cell types—according to two complementary enrichment analysis approaches (Methods and Supplementary Fig. 9)—with strong enrichment observed in stimulated CD4+ effector T cells (Supplementary Fig. 9b). There was no enrichment in pancreatic islets ($P = 0.14$), the primary target of autoimmunity in T1D—even after exposure to pro-inflammatory cytokines ($P = 0.05$)—or cardiac fibroblasts ($P > 0.60$; Supplementary Fig. 9). We also examined enrichment for T1D credible variants in condition-specific accessible chromatin and

Table 2 | T1D associations co-localizing with caQTLs in CD4$^+$ T cells

T1D lead variant[a]	β_{T1D}[b]	Peak	T1D credible variants in peak	caQTL lead variant[a]	β_{caQTL}[b]	P_{caQTL}	PP	Whole-blood *cis*-eQTLs[c]
rs71624119 (chr5:56144903:G:A)	−0.099	chr5:56147972–56149111	rs7731626	rs7731626 (chr5:56148856:G>A)	−0.5	2.4×10^{-9}	0.97	*ANKRD55* ($z=-58$; PP = 0.98) *IL6ST* ($z=-10$; PP = 0.98)
rs72928038 (chr6:90267049:G:A)	0.172	chr6:90266766–90267747	rs72928038	rs72928038 (chr6:90267049:G>A)	−1.0	3.9×10^{-16}	1.00	*BACH2* ($z=-21$; PP = 1)
rs2027299 (chr6:126364681:G:C)	0.147	chr6:126339725–126340580	rs9388486	rs1361262 (chr6:126380821:T>C)	−0.4	2.0×10^{-16}	0.87	*CENPW* ($z=-9.8$; PP = 0.82)
rs61555617[d] (chr12:56047884:TA:T)	0.257	chr12:56041256–56042638	rs705704 rs705705	rs705704 (chr12:56041628:G>A)	−0.2	1.1×10^{-15}	0.97	*GDF11* ($z=-7.5$[e]; PP = 0.97)
rs4900384 (chr14:98032614:A:G)	0.118	chr14:98018322–98019163	rs11628807 rs4383076 rs11628876 rs11160429	rs11628807 (chr14:98018774:T>G)	0.7	1.8×10^{-21}	0.95	-

Five regions show co-localization between T1D and a caQTL with a co-localization posterior probability > 0.8. In all of these regions, at least one T1D credible variant overlaps the caQTL peak itself. In four regions, the T1D association also co-localizes with an eQTL for expression of one or more genes in whole blood. [a]The T1D lead variant is the most-associated variant in the credible set, as defined by fine mapping (Supplementary Table 11); the caQTL lead variant is the most-associated variant with chromatin accessibility at the peak of interest. Variants are provided as rsid (chromosome:hg38_position:reference:alternative). [b]β_{T1D} refers to the effect size for the alternative allele of the T1D lead variant and β_{caQTL} refers to the effect size for the alternative allele of the caQTL lead variant. [c]Whole-blood *cis*-eQTL statistics from eQTLGen for the T1D lead variant and co-localization with the T1D association. [d]rs61555617 is referred to as rs796916887 in the Supplementary tables. [e]The *cis*-eQTL statistics for rs61555617 are missing in eQTLGen; the reported *GDF11 cis*-eQTL *z*-score is for the highly correlated variant rs705704. PP, posterior probability of co-localization between the QTL (eQTL or caQTL) and the T1D association (referred to in coloc documentation as 'PP.H4.abf').

observed the largest enrichment in stimulation-specific peaks from effector CD4$^+$ T cells (Supplementary Note, Supplementary Table 14 and Supplementary Fig. 10).

Co-localization of T1D association with QTLs in immune cells. Chromatin-accessibility profiles were generated across 115 participants ($n_{EUR}=48$ and $n_{AFR}=67$) in primary CD4$^+$ T cells, the cell type in which accessible chromatin is most strongly enriched for T1D credible variants (Supplementary Figs. 9 and 10). We examined the additive effects of genotype on local chromatin accessibility (*cis* window < 1 Mb), thereby identifying 11 'peaks' of chromatin accessibility that were significantly ($P<5\times10^{-5}$) associated with T1D credible variants. Co-localization analysis of T1D association and caQTLs (R package coloc[41]; Methods) identified five regions supporting a common causal variant underlying association with T1D and chromatin accessibility (PP.H4.abf > 0.8; Table 2). At least one T1D credible variant overlapped the caQTL-associated peak in all five regions. Six of these 'within-peak' credible variants were directly genotyped on the ImmunoChip, allowing us to examine allele-specific accessibility in heterozygous participants (Methods). For all six variants, the proportion of ATAC-seq reads from heterozygotes containing the alternative allele was consistent with the direction of the caQTL effect (Supplementary Table 15). When integrated with whole-blood *cis*-expression quantitative trait loci (eQTLs)[41,42], co-localization identified T1D candidate genes in four of five T1D-caQTL regions (PP.H4.abf > 0.8; Table 2).

Functional annotation of T1D-associated variants in the *BACH2* region. Fine mapping of the *BACH2* locus refined the T1D association to two intronic variants, rs72928038 (NC_000006.12:g.90267049G>A) and rs6908626 (NC_000006.12:g.90296024G > T; Fig. 3a). The EUR minor alleles of rs72928038:G>A and rs6908626:G>T are associated with increased T1D risk (OR = 1.18, $P<1\times10^{-20}$, $MAF_{EUR}=0.18$). Chromatin-state annotations across cell types from the BLUEPRINT Consortium and National Institutes of Health (NIH) Roadmap Epigenomics Project annotate rs72928038:G>A as overlapping a T cell–specific active enhancer and rs6908626:G>T as lying in the ubiquitous *BACH2* promoter (Fig. 3b). Promoter-capture Hi-C data from diverse immune-cell types[43] indicate that the enhancer region containing rs72928038:G>A contacts the *BACH2* promoter in T cells (Fig. 3c). Although weak interactions were observed in multiple T-cell subtypes, only naive CD4$^+$ T cells had a significant interaction score.

In the caQTL analysis, rs72928038:G>A was associated with decreased accessibility of the enhancer it overlaps (chr6:90266766–90267715; Fig. 3d, left), whereas rs6908626:G>T did not affect accessibility at the *BACH2* promoter (chr6:90294665–90297341; Fig. 3d, right). Similarly, among 14 subjects heterozygous for rs72928038:G>A, only 4% (5/121) of ATAC-seq reads overlapping that site contained the T1D risk allele (A; Fig. 3e, left and Supplementary Table 15), suggesting it leads to restricted accessibility. In contrast, chromatin accessibility at rs6908626:G>T did not exhibit allelic bias in heterozygotes (Fig. 3e, right). These data help to prioritize rs72928038:G>A, rather than rs6908626:G>T, as functionally relevant in CD4$^+$ T cells.

In eQTL studies, rs72928038:G>A is associated with decreased expression of *BACH2* in whole blood[42] and purified immune-cell types[44]. In the DICE consortium[44], rs72928038:G>A is associated with decreased expression of *BACH2* in multiple cell types, with the strongest effects observed in naive CD4$^+$ and CD8$^+$ T cells. This result is consistent with the observation that the enhancer region overlapping rs72928038:G>A is accessible specifically in unstimulated bulk CD4$^+$, unstimulated bulk CD8$^+$ and naive CD4$^+$ T effector cells (Fig. 3f). Both the enhancer caQTL and *BACH2* eQTL co-localize with T1D association (Fig. 3g and Table 2).

The *BACH2* rs72928038:G>A variant overlaps binding sites for STAT1 and the ETS family of transcription factors, based on canonical transcription-factor binding motifs[33]. We performed supershift electrophoretic mobility shift assay (EMSA) experiments of the DNA sequence flanking rs72928038:G>A that demonstrated allele-specific ETS1 binding but no STAT1 binding (Supplementary Fig. 11). This result builds on experiments demonstrating allele-specific nuclear protein binding of rs72928038:G>A in Jurkat cells[45]. These data prioritize rs72928038:G>A as a probable functional variant in T cells and provide preliminary support for a candidate regulatory mechanism underlying the 6q15 region association with T1D. Specifically, we hypothesize that the rs72928038:G>A minor allele (A) disrupts ETS1 binding, which leads to decreased enhancer activity and *BACH2* expression in naive CD4$^+$ T cells.

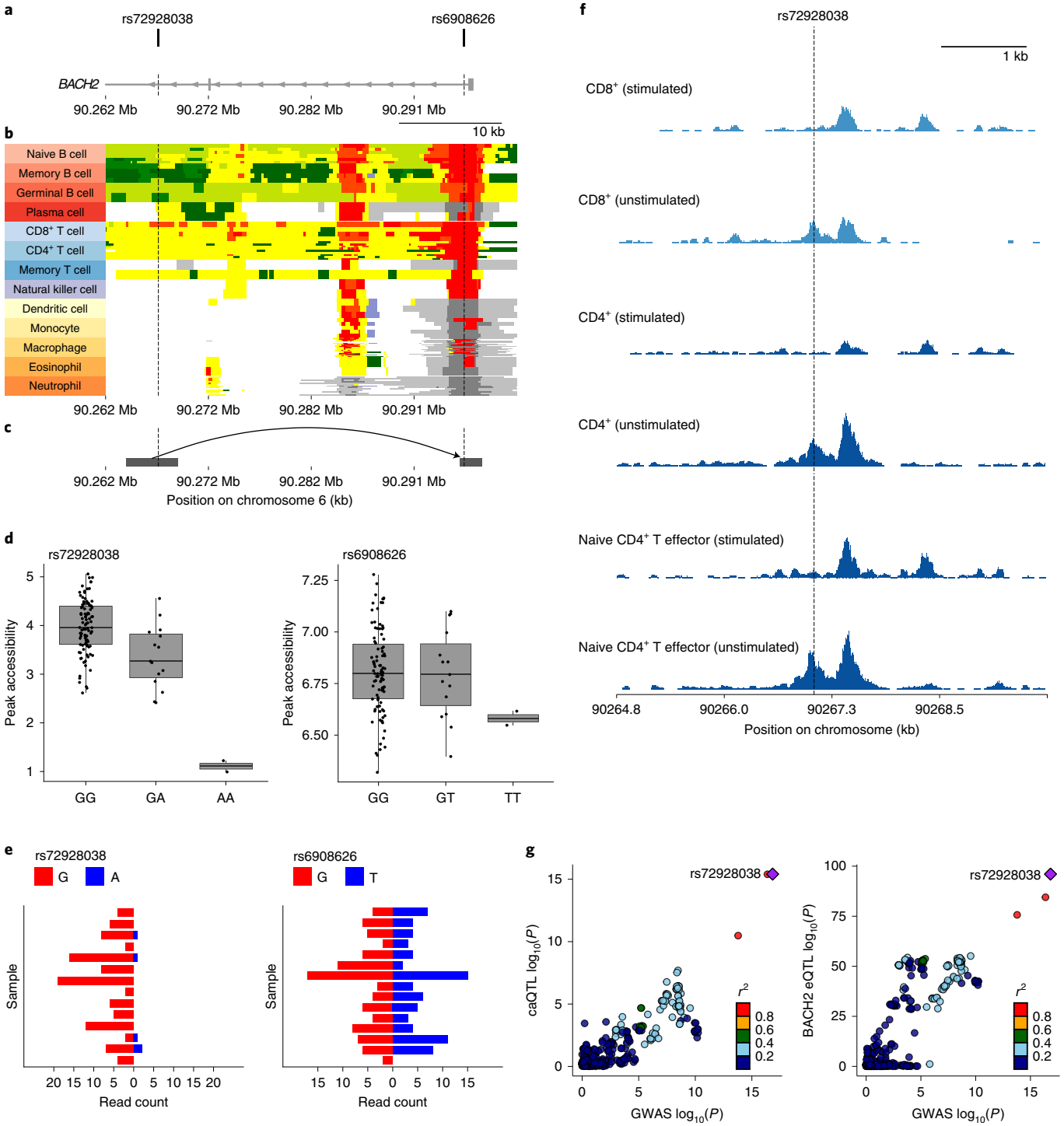

Fig. 3 | Functional annotation of T1D-associated variants in the *BACH2* region. a–**c**, Position of T1D credible variants (rs72928038:G>A and rs6908626:G>T) relative to the introns and exons of *BACH2* (**a**), chromHMM tracks across diverse immune-cell types from the BLUEPRINT consortium (**b**; red, active promoter; orange, distal active promoter; dark green, transcription; light green, genic enhancer; yellow, enhancer; white, quiescent; light gray, Polycomb repressed; dark gray, repressed; and blue, heterochromatin) and interactions with the *BACH2* promoter in published PCHi-C data from naive CD4+ T cells[43] (**c**; the gray squares indicate boundaries of target (left) and bait (right)). The chromatin coordinates and the scale are identical and aligned. **d**, Accessibility of regions overlapping rs72928038:G>A (left) and rs6908626:G>T (right) according to genotype. Peak accessibility is quantified as the normalized transposase cut frequency (Methods); center line, median; box limits, upper and lower quartiles; whiskers, 1.5× the interquartile range ($n=115$ individuals). **e**, Allele-specific accessibility of chromatin within heterozygous individuals at rs72928038:G>A (left; $n=14$ heterozygous individuals) and rs6908626:G>T (right; $n=15$ heterozygous individuals). **f**, Chromatin-accessibility profiles in the region overlapping rs72928038:G>A across resting and activated CD4+ and CD8+ T cells (published data[38]). The height of the tracks represents the transposase cut frequency; all tracks are plotted using the same vertical scale. **g**, LocusCompare plots showing co-localization between T1D association, the caQTL for chr6:90266766–90267715 (left) and the eQTL for *BACH2* (right).

T1D drug-target identification. To identify potential T1D therapeutic targets with human genetic support, we used the priority-index algorithm[46], which integrates genetic association results with genome annotations, regulatory maps and protein–protein networks (Methods). Using improved T1D-association statistics and additional eQTL resources from whole blood[42], we identified 50 highly ranked gene targets (Supplementary Table 16). These targets include 26 'seed genes' (implicated by T1D-associated loci through proximity, eQTL effects or chromatin looping) and 24 non-seed genes (not in T1D regions but highly connected to T1D seed genes in immune protein networks). Although we excluded variants in the MHC region from algorithm input, the networks implicated by non-MHC seed genes led to prioritization of *HLA-DRB1*, an established T1D risk factor. Among the top-50 gene targets, 13 were not previously implicated by priority-index analyses (*STAT4*, *RGS1*, *CXCR6*, *IL23A*, *PTPN22*, *NFKB1*, *MAPK3*, *EPOR*, *DGKQ*, *GALT*, *IL12RB1*, *IL12RB2* and *IL6R*)[46], and 12 have been targeted in clinical trials for autoimmune diseases (*IL2RA*, *IL6ST*, *IL6R*, *TYK2*, *IFNAR2*, *JAK2*, *IL12B*, *IL23A*, *IL2RG*, *JAK3*, *JAK1* and *IL2RB*). T1D susceptibility alleles may alter the expression of gene targets in either direction, and gene regulatory effects may be seen across multiple major immune-cell populations or be restricted to a single cell type (Supplementary Fig. 12). For example, T1D risk alleles are associated with increased expression of *MAPK3* and *DGKQ* but decreased expression of *TYK2* across multiple major immune-cell populations. In contrast, risk alleles decrease the expression of *RGS1* across most immune-cell types but increase expression specifically in CD8$^+$ T cells. The directionality and cell-type specificity of gene regulatory effects associated with T1D risk alleles may inform therapeutic target considerations.

Discussion

In the largest genetic analysis of T1D to date, we identified 36 new regions at genome-wide significance and implicated a total of 152 regions outside the MHC in T1D susceptibility at FDR < 0.01. We refined the set of putative causal variants and number of independent associations in many T1D regions through increased sample size, dense genotyping and imputation, inclusion of diverse ancestry groups and optimized analytical approaches to fine mapping. We assessed the intersection of T1D-associated variants with regions of putative regulatory function with public and newly generated ATAC-seq data from diverse cell types and states, demonstrating that T1D credible variants were enriched in stimulation-responsive open-chromatin peaks in CD4$^+$ T cells. We assessed the co-localization of the T1D associations with CD4$^+$ T-cell caQTLs to generate mechanistic hypotheses centered on this highly relevant cell type. Finally, we identified potential T1D drug targets for use in prevention trials. Experimental follow-up studies are required to test these hypotheses and further dissect the mechanisms altering T1D risk in each region.

Despite the enrichment of credible variants in CD4$^+$ T-cell open chromatin, only five of 52 fine-mapped T1D associations could be explained by a co-localized caQTL. This result is consistent with work exploring the functional effects of variants associated with immune traits[47]. One explanation is limited power in QTL discovery due to small sample sizes or imprecise cell types[47,48]. The analysis of more refined cell types—for example, using single-cell approaches—for both enrichment analyses and QTL discovery may lead to additional discoveries[49,50]. Nevertheless, although this approach may lack sensitivity, the five regions showing co-localization between caQTL and T1D associations prioritize variants with regulatory effects that represent realistic targets for experimental follow-up. In particular, within-peak credible variants with consistent caQTL effects and allele-specific accessibility, although not definitively causal, provide high-priority candidate variants for functional follow-up. As four of the five T1D associations that co-localize with caQTLs also co-localize with whole-blood eQTLs, these regions offer hypotheses for how causal variants influence disease risk through their effects on regulatory-element activity and gene expression in T1D-relevent cell types.

In the 5q11.2 region, fine mapping and caQTL co-localization point to the within-peak variant rs7731626 (NC_000005.10:g.56148856G>A) as a potential causal variant for T1D. This result complements a recent regulatory QTL fine-mapping study that highlighted the same variant as likely to be functional in T cells[51]. In addition, the T1D association co-localizes with eQTLs for both *ANKRD55* and *IL6ST*, mirroring results in multiple sclerosis, Crohn's disease and rheumatoid arthritis[47]. The region overlapping rs7731626:G>A loops to the *IL6ST* promoter in CD4$^+$ T cells, according to promoter-capture Hi-C data[43]. Although we did not find evidence that rs7731626:G>A loops to the canonical transcription start site for *ANKRD55*, nascent RNA-sequencing data suggest it overlaps the 5′ end of the transcriptionally active region of *ANKRD55* in human T cells[52], consistent with a potential regulatory role.

We highlight the *BACH2* region on chromosome 6q15 as an example of unbiased QTL co-localization that leads to hypotheses for functional mechanisms driving variant-T1D association. We hypothesize that rs72928038:G>A, the T1D-associated allele, abolishes ETS1 binding at an enhancer that promotes *BACH2* expression in naive CD4$^+$ T cells. *BACH2* encodes the transcription factor from the BTB-basic leucine zipper family BACH2, which has established roles in B- and T-cell biology, including maintenance of the naive T-cell state[53,54]. *BACH2* haploinsufficiency has been shown to cause congenital autoimmunity and immunodeficiency[55], demonstrating that a functioning human immune system depends on *BACH2* expression in a dose-dependent manner. In addition to *cis*-effects on *BACH2* expression, rs72928038:G>A is associated with altered expression of 39 distal genes[42] in whole blood, including seven genes in autoimmune disease-associated regions. These observations raise the hypothesis that the minor A allele at rs72928038:G>A increases T1D risk by reducing *BACH2* expression in a precise cellular context (for example, the naive T-cell state). This effect may lead to shifts in BACH2-regulated transcriptional programs, thereby altering T cell lineage differentiation in response to antigen exposure.

Previous studies demonstrated shared genetic risk across autoimmune diseases[3,56] and suggest the potential for repurposing drugs to treat or prevent T1D. Our priority-index analysis identified 12 targets that have been the focus of clinical trials for the treatment of autoimmune diseases. One example is *IL23A*, which has been successfully targeted in the treatment of inflammatory bowel disease[57] and psoriasis[58]. The IL-23 inhibitors are being explored for use in T1D (ClinicalTrials.gov identifiers NCT02204397 and NCT03941132). Our results provide genetic support for these trials. Similarly, *JAK1*, *JAK2* and *JAK3* were implicated in T1D etiology in our analysis. JAK inhibitors are safe and effective in the treatment of rheumatoid arthritis[59] and ulcerative colitis[60]. Finally, this study presents the first well-powered convincing genetic evidence linking interleukin-6 (IL-6), a cytokine with known roles in multiple autoimmune diseases, to T1D etiology. The IL-6R complex consists of two essential subunits: the alpha subunit (encoded by *IL6R*) and the signal-transducing subunit (encoded by *IL6ST*). Both the *IL6ST* and *IL6R* regions were identified here as T1D-associated at genome-wide significance (Table 1), and both *IL6ST* and *IL6R* were prioritized by the priority-index analysis. *IL6ST* is implicated by QTL co-localization and the lead T1D variant near *IL6R* (rs2229238:T>C) is an eQTL for *IL6R* expression in whole blood (formal co-localization was not assessed as the *IL6R* region is not densely covered by the ImmunoChip). Based on the current evidence, we cannot say that *IL6ST* and *IL6R* are T1D causal genes. The associations in each region may be unrelated and due to different causal genes—for example, the association near *IL6ST* also co-localizes with an eQTL for *ANKRD55*. However, we note that the humanized IL-6R antagonist monoclonal antibody tocilizumab

is an approved treatment for rheumatoid arthritis and systemic juvenile idiopathic arthritis, both of which share substantial genetic effects with T1D[3] (Supplementary Fig. 7), and a trial of this drug in recently diagnosed T1D cases is underway (ClinicalTrials.gov identifier NCT02293837). Surprisingly, we showed that the lead T1D variant near *IL6R* (rs2229238:T>C) tags a causal variant distinct from the nonsynonymous variant in *IL6R*, rs2228145:A>C (NP_000556.1:p.Asp358Ala), that is thought to drive the association in rheumatoid arthritis[26], suggesting potentially different mechanisms altering disease risk in this region. The recent success of anti-CD3 therapy, after 40 years of study through experimental models and clinical trials targeting different patient subgroups and time points relative to disease diagnosis[61], highlights both the challenges and hopes for translating target identification to efficacious clinical outcomes in T1D.

One limitation of this study is that genotyping was restricted to ImmunoChip content, which provides dense coverage in 188 immune-relevant genomic regions, as defined by previous largely EUR ancestry-based genome-wide association studies (GWAS) of immune-related traits. This design restricts the scope of discovery, fine mapping and generalizability of subsequent functional enrichment analyses. This may explain the absence of T1D-variant enrichment in the open chromatin of non-immune-cell types (for example, pancreatic islets)[62,63]. In addition, the effect sizes of new loci are likely to have been overestimated due to winner's curse, particularly those identified in the groups of non-EUR ancestry (where the sample sizes remain small) such as rs190514104:G>A near *MTF1*. We also acknowledge the possibility of the results for the non-EUR ancestry groups being confounded by admixture. Although this analysis is the largest and most comprehensive study prioritizing new gene targets in T1D according to genetic evidence, extension of future genetic studies to genome-wide analyses[28] and continuing efforts to expand cohorts from diverse populations will further define the genetic landscape of T1D.

Online content

Any methods, additional references, Nature Research reporting summaries, source data, extended data, supplementary information, acknowledgements, peer review information; details of author contributions and competing interests; and statements of data and code availability are available at https://doi.org/10.1038/s41588-021-00880-5.

Received: 19 June 2020; Accepted: 5 May 2021;
Published online: 14 June 2021

References

1. Barrett, J. C. et al. Genome-wide association study and meta-analysis find that over 40 loci affect risk of type 1 diabetes. *Nat. Genet.* **41**, 703–707 (2009).
2. Todd, J. A. et al. Robust associations of four new chromosome regions from genome-wide analyses of type 1 diabetes. *Nat. Genet.* **39**, 857–864 (2007).
3. Onengut-Gumuscu, S. et al. Fine mapping of type 1 diabetes susceptibility loci and evidence for colocalization of causal variants with lymphoid gene enhancers. *Nat. Genet.* **47**, 381–386 (2015).
4. Inshaw, J. R. J., Walker, N. M., Wallace, C., Bottolo, L. & Todd, J. A. The chromosome 6q22.33 region is associated with age at diagnosis of type 1 diabetes and disease risk in those diagnosed under 5 years of age. *Diabetologia* **61**, 147–157 (2018).
5. Fortune, M. D. et al. Statistical colocalization of genetic risk variants for related autoimmune diseases in the context of common controls. *Nat. Genet.* **47**, 839–846 (2015).
6. Evangelou, M. et al. A method for gene-based pathway analysis using genomewide association study summary statistics reveals nine new type 1 diabetes associations. *Genet. Epidemiol.* **38**, 661–670 (2014).
7. Rewers, M. & Ludvigsson, J. Environmental risk factors for type 1 diabetes. *Lancet* **387**, 2340–2348 (2016).
8. Sharp, S. A. et al. Development and standardization of an improved type 1 diabetes genetic risk score for use in newborn screening and incident diagnosis. *Diabetes Care* **42**, 200–207 (2019).
9. Krischer, J. P. et al. Predicting islet cell autoimmunity and type 1 diabetes: an 8-year TEDDY Study progress report. *Diabetes Care* **42**, 1051–1060 (2019).
10. Onengut-Gumuscu, S. et al. Type 1 diabetes risk in African-ancestry participants and utility of an ancestry-specific genetic risk score. *Diabetes Care* **42**, 406–415 (2019).
11. Skyler, J. S. Hope vs hype: where are we in type 1 diabetes? *Diabetologia* **61**, 509–516 (2018).
12. Herold, K. C. et al. An anti-CD3 antibody, teplizumab, in relatives at risk for type 1 diabetes. *N. Engl. J. Med.* **381**, 603–613 (2020).
13. King, E. A., Davis, J. W. & Degner, J. F. Are drug targets with genetic support twice as likely to be approved? Revised estimates of the impact of genetic support for drug mechanisms on the probability of drug approval. *PLoS Genet.* **15**, e1008489 (2019).
14. Nelson, M. R. et al. The support of human genetic evidence for approved drug indications. *Nat. Genet.* **47**, 856–860 (2015).
15. Wellcome Trust Case Control Consortium. Genome-wide association study of 14,000 cases of seven common diseases and 3,000 shared controls. *Nature* **447**, 661–678 (2007).
16. Cooper, J. D. et al. Meta-analysis of genome-wide association study data identifies additional type 1 diabetes risk loci. *Nat. Genet.* **40**, 1399–1401 (2008).
17. Hakonarson, H. et al. A novel susceptibility locus for type 1 diabetes on Chr12q13 identified by a genome-wide association study. *Diabetes* **57**, 1143–1146 (2008).
18. Grant, S. F. A. et al. Follow-up analysis of genome-wide association data identifies novel loci for type 1 diabetes. *Diabetes* **58**, 290–295 (2009).
19. Bradfield, J. P. et al. A genome-wide meta-analysis of six type 1 diabetes cohorts identifies multiple associated loci. *PLoS Genet.* **7**, e1002293 (2011).
20. Huang, J., Ellinghaus, D., Franke, A., Howie, B. & Li, Y. 1000 Genomes-based imputation identifies novel and refined associations for the Wellcome Trust Case Control Consortium phase 1 Data. *Eur. J. Hum. Genet.* **20**, 801–805 (2012).
21. Zhu, M. et al. Identification of novel T1D risk loci and their association with age and islet function at diagnosis in autoantibody-positive T1D individuals: based on a two-stage genome-wide association study. *Diabetes Care* **42**, 1414–1421 (2019).
22. Divers, J. et al. Trends in incidence of type 1 and type 2 diabetes among youths—selected counties and Indian reservations, United States, 2002–2015. *Morb. Mortal. Wkly Rep.* **69**, 161–165 (2020).
23. Taliun, D. et al. Sequencing of 53,831 diverse genomes from the NHLBI TOPMed Program. *Nature* **590**, 290–299 (2021).
24. Cortes, A. et al. Promise and pitfalls of the Immunochip. *Arthritis Res. Ther.* **13**, 101 (2011).
25. Ferreira, R. C. et al. Functional *IL6R* 358Ala allele impairs classical IL-6 receptor signaling and influences risk of diverse inflammatory diseases. *PLoS Genet.* **9**, e1003444 (2013).
26. Okada, Y., Wu, D., Trynka, G. & Towfique, R. Genetics of rheumatoid arthritis contributes to biology and drug discovery. *Nature* **506**, 376–381 (2014).
27. Benjamini, Y. & Yekutieli, D. The control of the false discovery rate in multiple testing under depencency. *Ann. Stat.* **29**, 1165–1188 (2001).
28. Crouch, D. J. M. et al. Enhanced genetic analysis of type 1 diabetes by selecting variants on both effect size and significance, and by integration with autoimmune thyroid disease. Preprint at *bioRxiv* https://doi.org/10.1101/2021.02.05.429962 (2021).
29. Wallace, C. et al. Dissection of a complex disease susceptibility region using a Bayesian stochastic search approach to fine mapping. *PLoS Genet.* **11**, e1005272 (2015).
30. Asimit, J. L. et al. Stochastic search and joint fine-mapping increases accuracy and identifies previously unreported associations in immune-mediated diseases. *Nat. Commun.* **10**, 3216 (2019).
31. Wojcik, G. L. et al. Genetic analyses of diverse populations improves discovery for complex traits. *Nature* **570**, 514–518 (2019).
32. Kichaev, G. & Pasaniuc, B. Leveraging functional-annotation data in trans-ethnic fine-mapping studies. *Am. J. Hum. Genet.* **97**, 260–271 (2015).
33. Boyle, A. P. et al. Annotation of functional variation in personal genomes using RegulomeDB. *Genome Res.* **22**, 1790–1797 (2012).
34. Lizio, M. et al. Gateways to the FANTOM5 promoter level mammalian expression atlas. *Genome Biol.* **16**, 22 (2015).
35. Ramos-rodríguez, M. et al. The impact of proinflammatory cytokines on the β-cell regulatory landscape provides insights into the genetics of type 1 diabetes. *Nat. Genet.* **51**, 1588–1595 (2019).
36. Ward, L. D. & Kellis, M. HaploReg v4: systematic mining of putative causal variants, cell types, regulators and target genes for human complex traits and disease. *Nucleic Acids Res.* **44**, 877–881 (2016).
37. Buenrostro, J. D., Wu, B., Chang, H. Y. & Greenleaf, W. J. ATAC-seq: a method for assaying chromatin accessibility genome-wide. *Curr. Protoc. Mol. Biol.* **109**, 21.29.1–21.29.9 (2015).

38. Calderon, D. et al. Landscape of stimulation-responsive chromatin across diverse human immune cells. *Nat. Genet.* **51**, 1494–1505 (2019).
39. Varshney, A. et al. Genetic regulatory signatures underlying islet gene expression and type 2 diabetes. *Proc. Natl Acad. Sci. USA* **114**, 2301–2306 (2017).
40. Jonsson, M. K. B. et al. A transcriptomic and epigenomic comparison of fetal and adult human cardiac fibroblasts reveals novel key transcription factors in adult cardiac fibroblasts. *JACC Basic Transl. Sci.* **1**, 590–602 (2016).
41. Giambartolomei, C. et al. Bayesian test for colocalisation between pairs of genetic association studies using summary statistics. *PLoS Genet.* **10**, e1004383 (2014).
42. Võsa, U. et al. Unraveling the polygenic architecture of complex traits using blood eQTL meta-analysis. Preprint at *bioRxiv* https://doi.org/10.1101/447367 (2018).
43. Javierre, B. M. et al. Lineage-specific genome architecture links enhancers and non-coding disease variants to target gene promoters. *Cell* **167**, 1369–1384 (2016).
44. Schmiedel, B. J. et al. Impact of genetic polymorphisms on human immune cell gene expression. *Cell* **175**, 1701–1715 (2018).
45. Westra, H. J. et al. Fine-mapping and functional studies highlight potential causal variants for rheumatoid arthritis and type 1 diabetes. *Nat. Genet.* **50**, 1366–1374 (2018).
46. Fang, H. et al. A genetics-led approach defines the drug target landscape of 30 immune-related traits. *Nat. Genet.* **51**, 1082–1091 (2019).
47. Chun, S. et al. Limited statistical evidence for shared genetic effects of eQTLs and autoimmune-disease-associated loci in three major immune-cell types. *Nat. Genet.* **49**, 600–605 (2017).
48. Hukku, A. et al. Probabilistic colocalization of genetic variants from complex and molecular traits: promise and limitations. *Am. J. Hum. Genet.* **108**, 25–35 (2021).
49. Chiou, J. et al. Interpreting type 1 diabetes risk with genetics and single-cell epigenomics. *Nature* https://doi.org/10.1038/s41586-021-03552-w (2021).
50. Benaglio, P. et al. Mapping genetic effects on cell type-specific chromatin accessibility and annotating complex trait variants using single nucleus ATAC-seq. Preprint at *bioRxiv* https://doi.org/10.1101/2020.12.03.387894 (2020).
51. Kundu, K. et al. Genetic associations at regulatory phenotypes improve fine-mapping of causal variants for twelve immune-mediated diseases. Preprint at *bioRxiv* https://doi.org/10.1101/2020.01.15.907436 (2020).
52. Danko, C. G. et al. Dynamic evolution of regulatory element ensembles in primate CD4$^+$ T cells. *Nat. Ecol. Evol.* **2**, 537–548 (2018).
53. Tsukumo, S. et al. Bach2 maintains T cells in a naive state by suppressing effector memory-related genes. *Proc. Natl Acad. Sci. USA* **110**, 10735–10740 (2013).
54. Roychoudhuri, R. et al. BACH2 regulates CD8$^+$ T cell differentiation by controlling access of AP-1 factors to enhancers. *Nat. Immunol.* **17**, 851–860 (2016).
55. Afzali, B. et al. BACH2 immunodeficiency illustrates an association between super-enhancers and haploinsufficiency. *Nat. Immunol.* **18**, 813–823 (2017).
56. Cotsapas, C. et al. Pervasive sharing of genetic effects in autoimmune disease. *PLoS Genet.* **7**, e1002254 (2011).
57. Faegan, B. G. et al. Risankizumab in patients with moderate to severe Crohn's disease: an open-label extension study. *Lancet Gastroenterol. Hepatol.* **3**, 671–680 (2018).
58. Fotiadou, C., Lazaridou, E., Sotiriou, E. & Ioannides, D. Targeting IL-23 in psoriasis: current perspectives. *Psoriasis Targets Ther.* **8**, 1–5 (2018).
59. Wollenhaupt, J. et al. Safety and efficacy of tofacitinib for up to 9.5 years in the treatment of rheumatoid arthritis: final results of a global, open-label, long-term extension study. *Arthritis Res. Ther.* **21**, 89 (2019).
60. Sandborn, W. J. et al. Tofacitinib as induction and maintenance therapy for ulcerative colitis. *N. Engl. J. Med.* **376**, 1723–1736 (2017).
61. Gaglia, J. & Kissler, S. Anti-CD3 antibody for the prevention of type 1 diabetes: a story of perseverance. *Biochemistry* **58**, 4107–4111 (2019).
62. Aylward, A., Chiou, J., Okino, M.-L., Kadakia, N. & Gaulton, K. J. Shared genetic risk contributes to type 1 and type 2 diabetes etiology. *Hum. Mol. Genet.* https://doi.org/10.1093/hmg/ddy314 (2018).
63. Dooley, J. et al. Genetic predisposition for beta cell fragility underlies type 1 and type 2 diabetes. *Nat. Genet.* **48**, 519–527 (2016).

Type 1 Diabetes Genetics Consortium

Patrick Concannon[18,27], Flemming Pociot[21,22,23], Stephen S. Rich[1,4] and John A. Todd[3]

Methods

Genotyping and quality control. The DNA samples were genotyped on the Illumina ImmunoChip at the University of Virginia (UVA) Genome Sciences Laboratory ($n=52,219$), Sanger Institute ($n=4,347$), University of Cambridge ($n=2,941$) and Feinstein Institute ($n=1,811$). Raw genotyping files were assembled at the UVA. Genotype clusters were generated using the Illumina GeneTrain2 algorithm. Stringent SNP- and sample-level quality-control filtering and data cleaning were performed to ensure high-quality genotypes and accurate pedigrees (Supplementary Fig. 1). The following variant filters were applied: (1) re-annotation of ImmunoChip variant positions by aligning probe sequences to GRCh37 and the removal of any variants with <100% match or multiple matches at different positions in the genome; (2) removal of variants with call rates <98%; (3) removal of variants with any discordance between duplicate or monozygotic twin samples, as confirmed by genotype-inferred relationships; (4) removal of variants with Mendelian inconsistencies in >1% of the informative trios or parent–offspring pairs, based on genotype-inferred relationships.

For sample filtering, we used X-chromosome heterozygosity and Y-chromosome missingness to identify and exclude participants with apparent sex-chromosome anomalies or resolve inconsistencies with the reported sex. Pedigree-defined and genotype-inferred sample relationships were compared using KING version 2.1.3 (ref. [64]). Samples were excluded when inconsistencies could not be resolved, including relationships between families, within and across cohorts. For each pair of related families observed, we randomly selected one to remove from the association analysis. After resolving the sex and relationship issues, samples with a genotype call rate < 98% were removed. Variants with genotype frequencies deviating from Hardy–Weinberg equilibrium ($P<5\times10^{-5}$) in unrelated EUR-ancestry controls were excluded before imputation.

Stratification of major ancestry groups and family trios. Principal components were generated in 1000 Genomes phase-3 individuals using 8,297 autosomal ImmunoChip variants selected by excluding regions of long-range LD[65], pruning for short-range LD ($r^2<0.2$ in 50-kb windows) and filtering for MAF > 0.05. The participant genotypes were projected onto the 1000 Genomes principal-component space using PLINK v1.9 (ref. [66]). The first ten principal components were used in *k*-means clustering to define five clusters of ancestrally similar participants—EUR, AFR, EAS, FIN and AMR—labeled according to their closest 1000 Genomes super-population. For case-control analyses to be performed within each ancestry cluster, affected trios were excluded and a set of unrelated individuals was selected from the remaining subjects using KING version 2.1.3 software ('--unrelated' option)[64]. Cluster-specific principal components were calculated by performing principal-component analysis on unrelated controls and projecting the remaining subjects onto the resulting axes. The remaining population stratification within each ancestry cluster was assessed visually (Supplementary Fig. 3).

Defining targeted regions for discovery and fine-mapping analysis. The ImmunoChip densely covered genetic variation in the immune-associated genomic regions. Discovery analyses included all genotyped variants as well as imputed variants from any 500-kb region that contained more than 50 genotyped variants (Supplementary Table 3). To define boundaries for fine-mapping regions, we mapped previously defined ImmunoChip regions (provided by the R package humarray) from GRCh36 to GRCh38 coordinates (Supplementary Table 2): for each region, we mapped all variants originally included in the region to GRCh38 to define boundaries as the lowest and highest observed GRCh38 positions among these variants (±50 kb on either side). Fine-mapping analyses were then restricted to densely genotyped regions overlapping these ImmunoChip regions.

Association analysis. *Phase I: case-control analyses.* Genotypes were imputed with the National Heart, Lung and Blood Institute (NHLBI) TOPMed Freeze 5 (Supplementary Note) reference panel. We analyzed the association of all genotyped variants with T1D and high-confidence imputed variants separately in the five ancestry groups (Supplementary Tables 2,3 and Supplementary Note). Assuming an additive mode of inheritance, we used logistic regression for unrelated case-control analyses, adjusting for five ancestry-specific principal components and using genotype posterior probabilities to account for uncertainty in the imputed genotypes using the SNPTEST version 2.5.4 software[67]. Due to the small sample size (38 cases and 106 controls), the EAS individuals were excluded. We combined results using an inverse-variance weighted fixed-effects meta-analysis (METAL software version released on 25 March 2011)[68]. Forward stepwise logistic regression was performed to identify loci with more than one independent association with T1D. All conditionally independent associations ($P<5\times10^{-8}$) were reported. The case-control analyses were performed under recessive and dominant models of inheritance. To evaluate the relative fit of the three models, we compared the AIC in the EUR ancestry group and identified the model providing the lowest AIC (best fit). Only genotyped variants were examined for their association with T1D on the X chromosome. The Y chromosome was not examined.

Phase II: trio families and combined analyses. Trio families (two parents and an affected offspring) were analyzed within an ancestry group using the transmission-disequilibrium test[69]. As transmission disequilibrium test statistics are susceptible to substantial bias when applied to imputed genotypes[70], a stringent variant filter was applied to the imputed genotypes, removing all variants with Mendelian inconsistencies in >1% of trios with heterozygous offspring or parent–offspring pairs with homozygous offspring. From the transmission disequilibrium test summary statistics, we derived effect sizes and standard-error estimates[71] and meta-analyzed with the phase-I results.

Statistical fine mapping. Two complementary approaches were used to define credible variant sets within each T1D-associated ImmunoChip region. Fine mapping included high-confidence variants within 750 kb of the lead variant (1.5-Mb region in total), usually consisting of imputed variants across the entire ImmunoChip region and genotyped variants adjacent to the ImmunoChip region.

Fine mapping using EUR case-control data only. Given that forward stepwise model selection can fail to identify complex genetic architectures[30], we applied a Bayesian method (GUESSFM; see Supplementary Note) in the EUR case-control data to identify the most likely combinations of variants explaining T1D risk[29,72]. In the results we refer to groups of variants prioritized by GUESSFM as credible sets and variants within these groups as credible variants. Variants that failed the quality-control metrics (or were not genotyped or imputed in our data for other reasons) but were in LD ($r^2>0.9$ in 1000 Genomes Phase 3) with a prioritized variant were included in the comprehensive list of credible variants (Supplementary Table 11).

Trans-ancestry fine mapping. In regions where association signals were marginally associated ($P<5\times10^{-4}$) in multiple ancestry groups and evidence from EUR-ancestry-only fine mapping suggested a single causal variant (marginal posterior probability for one causal variant in the region > 0.5), we applied the multi-ancestry fine-mapping method PAINTOR[32] to refine the association. PAINTOR uses association *z*-scores and population-level LD to identify the combination of alleles that best explain the phenotype, multiplying the posterior probability of the causal vector across ancestry groups, assuming the same variant(s) are causal in each ancestry group. Given that the loci examined were those with evidence of one causal variant in the region, we restricted the maximum model size to two variants in the region and enumerated the posterior of every model, rather than performing a Markov-chain-Monte-Carlo search. The association *z*-scores used for each ancestry group were from a meta-analysis of case-controls and family trios in that ancestry cluster. PAINTOR input LD reference panels were generated separately for each ancestry group using LDstore version 1.1 (ref. [73]) using imputed genotype data from unrelated cases and controls.

Haplotype analyses. Haplotype analyses were performed in the EUR-ancestry cases and controls by taking 'best-guess' genotype values for the variants included in the analysis and obtaining haplotype phase-distribution estimates for each individual using an expectation-maximization algorithm[74]. The haplotype of each individual was sampled ten times and a logistic regression was fitted estimating the effect size of the haplotype relative to the most common haplotype in the population, with T1D status as the outcome and adjusting for five principal components. The estimates and standard errors for each haplotype relative to the most common were averaged over the ten logistic regression models to obtain the overall haplotype effect sizes on T1D risk.

Annotating T1D-associated protein-altering variants. The functional impacts of T1D credible variants (Supplementary Table 11) were annotated using ANNOVAR (version released on 16 April 2018)[75] and the Ensembl and refGene annotation databases.

Generating representative cell-type- and condition-specific chromatin-accessibility profiles. We downloaded publicly available ATAC-seq data from diverse immune-cell types[38], pancreatic islets[35] and cardiac fibroblasts[40] (see Data Availability).

We generated additional ATAC-seq data on $CD4^+$ T ($n=6$ donors) and $CD19^+$ B ($n=4$ donors) cells using different culture and stimulation conditions from Calderon and colleagues[38]. The $CD4^+$ T cells were enriched and stimulated as previously described[76]. The B cells were positively selected from peripheral blood mononuclear cells using anti-CD19 beads (Miltenyi Biotec, GmbH) and cultured for 24 h in X-VIVO 15 (Lonza) supplemented with 1% human Ab serum (Sigma) and penicillin–streptomycin (Thermo Fisher), and plated in 96-well CELLSTAR U-bottomed plates (Greiner Bio-One) at a concentration of 2.5×10^5 cells well^{-1}. The cells were left untreated or stimulated with 10 μg ml^{-1} goat anti-human IgM/IgG/IgA antibody (109-006-064, Jackson Immunoresearch), 0.15 μg ml^{-1} rhCD40L (ALX-522-110-C010, ENZO Lifesciences), and 20 ng ml^{-1} rhIL-21 and rhIL-4 (200-21 and 200-04, respectively, Peprotech) for 24 h. ATAC-seq data were generated from 50,000 cells from each cell type and culture condition following the Omni-ATAC protocol[77]. The ATAC-seq datasets were mapped to GRCh38.p12 (ref. [78]) using minimap2 (version 2.17)[79], except for GSE123404 (pancreatic-islets dataset), where bowtie2 (version 2.3.5) was used. After mapping, the technical replicates (where available) were merged and PCR-duplicated reads were detected using Picard tools (version 2.20.2). The percentage of detected duplicated reads was very low (mean value < 1%) in all datasets. Next, bigWig files

were generated using bamCoverage from the deeptools package (version 3.3.0), using reads-per-genome-coverage normalization and ignoring allosomes and the mitochondrial chromosome. Peaks were called using macs2 (version 2.1.2)[80] with the parameters '--nomodel --shift 37 --extsize 73 --keep-dup all'.

The immune-cell ATAC-seq dataset GSE118189 (ref. [38]) was used to create a consensus list of peaks. For each cell type, the donor contributing the fewest number of reads to that cell type was selected and the number of reads was divided by two. The reads were then randomly pooled by that number for each sample, creating a representative alignment file for that cell type. This procedure was performed twice to obtain two pseudo-replicates. Peaks were called using macs2 with the same parameters. The irreducible discovery rate (IDR) was calculated between the two pseudo-replicates[81], any peak with an IDR ≤ 0.05 were included in the consensus list of peaks. This list was then used as a feature reference and the reads were counted per feature using featureCounts from the package subread[82] (version 1.6.4). A similar approach was used for the other datasets in the analysis. The IDR was used to obtain a reliable list of peaks. In these datasets, no feature reference was derived from the IDR and counting was performed directly from the list obtained from GSE118189. Workflows were implemented using conda and snakemake.

ATAC-seq enrichment analyses. To examine the enrichment of T1D credible variants (group marginal posterior probability > 0.8 from GUESSFM) in open chromatin, two complementary approaches—SNP-matching and GoShifter[83] (http://software.broadinstitute.org/mpg/goshifter/)—were employed for each cell type. In the SNP-matching approach, the variants were randomly sampled across the genome and matched on LD structure and gene density to generate a null distribution of SNPs overlapping accessible chromatin ('SNP-matching enrichment analysis' section). GoShifter, in contrast, generates a null distribution within each locus (see Trynka et al.[83]).

SNP-matching enrichment analysis. The number of T1D credible variants falling within open chromatin was compared with variants in regions of the genome with similar LD structure and gene density as follows:

(1) Using EUR individuals from 1000 Genomes Project data, all variants with $r^2 > 0.8$ to each other were identified.
(2) The T1D credible variants with group marginal posterior probability > 0.8 were binned with regards to their LD block size: 1–9, 10–19, 20–49, 50–74,75–99,100–149 or 150–249.
(3) The 1000 Genomes Project data variants were binned with regards to LD block size, taking an LD block as the variants with $r^2 > 0.8$ with an index variant.
(4) For each T1D credible group, an LD block from the 1000 Genomes Project data of the same bin size and with the same (or similar for large haplotypes) number of genes overlapping the credible group was randomly selected; therefore, a similar number of variants to the T1D credible group with an approximately equivalent LD structure and gene density was selected.
(5) Repeated step (4) 100 times, yielding 100 randomly sampled genome segments with an approximately equivalent size and LD structure to the T1D credible variants.
(6) For cell type 'X', the number of T1D credible SNPs overlapping ATAC-seq peaks was counted. This was compared with the number overlapping ATAC-seq peaks from the first randomly sampled set of variants. The *z*-score (Fisher's exact test) was calculated for the comparison of ATAC-seq peak overlap with T1D credible variants versus randomly sampled variants with equivalent size, gene density and LD structure.
(7) Repeated step (6) 100 times, one for each randomly sampled set of haplotypes across the genome, thereby obtaining 100 *z*-scores.
(8) The mean *z*-score from the 100 tests was compared with a normal distribution to obtain an enrichment *P* value for cell type 'X'.

Steps (6)–(8) were performed for each cell type and condition.

Generating caQTL maps using T1DGC frozen samples. We profiled chromatin accessibility in 115 individuals (57 controls and 58 T1D cases; 67 AFR and 48 EUR) from the Type 1 Diabetes Genetics Consortium (T1DGC). $CD4^+$ T cells were purified from viably frozen peripheral blood mononuclear cells using magnetic cell separation according to the manufacturer's protocol, using either negative ($n = 42$; STEMCELL Technologies EasySep human $CD4^+$ T-cell isolation kit) or positive ($n = 73$; MACS Miltenyi Biotec) selection. The selection approach was incorporated in the data processing and analysis. After $CD4^+$ T-cell purification, the 'Omni-ATAC-seq' protocol[77] was followed for nuclei isolation, transposase incubation and library preparation. The libraries were sequenced using 75-bp paired-end reads on an Illumina NextSeq and data were processed using the PEPATAC pipeline[84]. Briefly, the reads were trimmed using Skewer (version0.2.2)[85] and, after removing reads mapping to mitochondrial and human repeat regions, were mapped to GRCh38 using bowtie2 (ref. [86]). The PCR duplicates were removed, enzyme cut sites were inferred based on read alignment and peaks were called using macs2 (ref. [80]). Libraries with transcription-start-site enrichment scores below 6 or fewer than 10×10^6 aligned reads were excluded from the analyses. A set of consensus peaks was determined by merging peaks across all samples using bedops (version 2.4.35)[87]. A matrix of peak counts was calculated by counting the number of cut sites within each consensus peak in each sample using the R package bigWig (https://github.com/andrelmartins/bigWig).

Peaks with low counts were excluded (required ≥10 reads in ≥50% of samples). Further peak quality filtering and normalization were performed using the R package edgeR[88]. These steps included:

(1) filtering for peaks with ≥10 counts per million across samples within each batch,
(2) peak-count normalization using the trimmed mean of M-values method[89],
(3) mean-variance modeling-based transformation using the 'voom' function to enable linear modeling of peak counts assuming a normal distribution, and
(4) removing outlier peaks by clustering samples based on the counts for each peak (one at a time using *k*-means with $k = 2$) and excluding any peak that resulted in one sample clustering separately from all of the other samples.

We confirmed matching sample identity between ATAC-seq libraries and genotyped individuals using the 'Match BAM to VCF' (MBV) command in the software tool set QTLtools[90]. Association between imputed genotype dosage and chromatin accessibility (caQTL analysis) was tested using a linear model, adjusting for the first two genotype principal components, age at sample collection, transcription-start-site enrichment score and $CD4^+$ T-cell purification approach using the R package MatrixEQTL[91]. The caQTL discovery analyses were performed separately by ancestry group (EUR and AFR) and combined in an inverse-variance-weighted fixed effect meta-analysis (R package meta). All variant-peak combinations were tested where the accessibility peak was within 1 Mb of a T1D credible variant.

Co-localization analysis. We evaluated co-localization of T1D and caQTL for all peaks where at least one T1D credible variant (as defined by GUESSFM) was associated with peak accessibility (meta-analysis $P < 5 \times 10^{-5}$) using the R package coloc[41] and visualized co-localized signals using the R package locuscomparer[92]. Conditional summary statistics were used in regions predicted to have more than one causal variant underlying the T1D association or regions with multiple, conditionally independent variants associated with accessibility of the same peak. When running coloc for T1D-caQTL co-localization, we used a prior probability of co-localization of 5×10^{-6} and provided association β and standard errors as input data. When running coloc for T1D–eQTL co-localization, we used the same priors and supplied association *z*-scores. We considered GWAS and QTL signals to be significantly co-localized when the posterior probability of co-localization was greater than 0.8 ('PP.H4.abf' > 0.8).

Allele-specific accessibility analysis. For significant caQTLs that co-localized with T1D-associated variants, we tested for allele-specific accessibility of the caQTL peak. First, we identified individuals heterozygous for T1D credible variants overlapping the caQTL peak. For each heterozygous individual, we then counted the number of reads overlapping the variant position containing the reference or alternative allele. We only performed this analysis if the T1D credible variant overlapping the caQTL peak was directly genotyped on the ImmunoChip, as uncertainty in the heterozygous status of an individual could lead to biased results. For peaks with at least five participants who had at least five reads overlapping the peak, we formally tested whether the proportion of reads containing an alternative allele deviated significantly from the expected null hypothesis proportion of 0.5. We calculated the *P* values for deviation from 'allelic balance' (proportion = 0.5 for each read) by fitting a generalized linear mixed model where the dependent variable is the number of reads and follows a Poisson distribution, and the independent variables include a fixed effect for the allele and a random effect for the participant.

Supershift EMSA. Jurkat cells (E6-1) were purchased from the American Type Culture Collection and cultured in RPMI-1640 medium (Gibco) supplemented with 10% fetal bovine serum, 1% penicillin–streptomycin and 1% sodium pyruvate at 37 °C and 5% CO_2.

Labeled (5′ IRDye 700) and unlabeled 31-bp, single-stranded oligonucleotides containing rs72928038 were obtained from Integrated DNA Technologies (reference allele strand, 5′-AGGGACGGATTTCCTGTAAGCTGATCTTGAA-3′; and alternative allele strand, 5′-AGGGACGGATTTCCTATAAGCTGATCTTGAA -3′) along with complementary oligonucleotides. Double-stranded oligonucleotides were generated by annealing equal amounts of labeled or unlabeled complementary oligonucleotides at 95 °C for 5 min, followed by gradual cooling with a ramp rate of −1.2 °C min^{-1} for 1 h (Bio-Rad C1000 Touch Thermal Cycler).

Nuclear extract from Jurkat cells was obtained by following the manufacturer's protocol for the NE-PER nuclear and cytoplasmic extraction reagents kit (Thermo Scientific) and the extracted nuclear protein was dialyzed with Slide-A-Lyzer MINI dialysis units, 10,000 MWCO (Thermo Scientific) against 1 l buffer (10 mM Tris, pH 7.5, 50 mM KCl, 200 mM NaCl, 1 mM dithiothreitol, 1 mM phenylmethylsulfonyl fluoride and 10% glycerol) for 16 h at 4 °C with slow stirring.

The binding reaction for the EMSA was carried out using 2 µl 10× binding buffer (100 mM Tris, 500 mM KCl and 10 mM dithiothreitol; pH 7.5), 2 µl of 25 mM dithiothreitol (2.5% Tween 20), 1 µl poly(dI-dC) (1 µg $µl^{-1}$ in 10 mM Tris and 1 mM EDTA; pH 7.5), 1 µl of 1% NP-40, 100 mM $MgCl_2$, 20 fmol IRDye double-stranded oligonucleotide probe and 16 µg Jurkat nuclear extract in a final volume of 20 µl.

For the supershift lanes, tested transcription-factor-binding antibodies (ETS1 rabbit mAb and Stat1 rabbit mAb) were diluted 1:50 with ddH_2O. Negative-control rabbit IgG was diluted to the same concentration as the tested antibody. Diluted antibody (1 µl) was added to the binding reaction mixture while maintaining a total volume of 20 µl. The binding reaction was incubated for 20 min at room temperature, after which 2 µl 10× Orange loading dye was added to the reaction. Electrophoresis was performed with binding reaction mixture on a pre-run 6% DNA retardation gel for 70 min at 70 V. To capture the image, the gel was placed directly on the Odyssey-CLx (Licor) scan bed. The gel was scanned with a thickness of 0.5 mm in the 700-nm channel. The EMSA binding condition for rs72928038 was repeated three times to ensure reproducibility of the experiment.

Priority index. To prioritize drug targets implicated by T1D genetic associations, we ran the priority-index algorithm, as implemented in the R package Pi[46]. Data used to identify eQTL co-localization (eGenes) included those from the initial publication (unstimulated monocytes[93], $n=414$; lipopolysaccharide-stimulated monocytes after 2 h (ref. [93]), $n=261$; lipopolysaccharide-stimulated monocytes after 24 h (ref. [93]), $n=322$; interferon-γ-stimulated monocytes after 24 h (ref. [93]), $n=367$; unstimulated B cells[94], $n=286$; unstimulated natural killer cells (unpublished), $n=245$; unstimulated neutrophils[95], $n=114$; unstimulated $CD4^+$ T cells[96], $n=293$; unstimulated $CD8^+$ T cells[96], $n=283$; and whole blood[97], $n=5{,}311$) as well as a larger whole-blood study ($n=31{,}684$)[42]. Hi-C data from monocytes, fetal thymus, naive $CD4^+$ T cells, total $CD4^+$ T cells, activated total $CD4^+$ T cells, non-activated total $CD4^+$ T cells, naive $CD8^+$ T cells, total $CD8^+$ T cells, naive B cells and total B cells[43] were used to identify genes interacting with index variants (cGenes). The data used to define functional genes (fGenes, pGenes and dGenes) were those used in the initial publication. The STRING database[98] was used to define protein–protein interaction networks, where a confidence score ≥ 700 was considered.

Statistical analyses. Unless otherwise noted, all statistical analyses and data visualization were performed using R version 3.6 (ref. [99]). All statistical tests based on symmetrically distributed test statistics were two-sided. No repeated measures data were analyzed in this study. All genotyped and ATAC-seq samples analyzed in the association tests represent distinct individuals. The R packages ggplot2, cowplot, ggbio, GenomicRanges, gridExtra, RColorBrewer and rtracklayer were used for data visualization.

Reporting Summary. Further information on research design is available in the Nature Research Reporting Summary linked to this article.

Data availability

All univariable summary statistics for genotype association with T1D (including imputed variants) are available through the NHGRI-EBI GWAS catalog (GCST90013445 and GCST90013446). The caQTL summary statistics are available through the Type 1 Diabetes Knowledge Portal (https://t1d.hugeamp.org).

Publicly available ATAC-seq: Raw FASTQ files were obtained from Gene Expression Omnibus (GEO) accession number GSE118189. These data included four individuals and 25 immune-cell types under resting conditions as well as after stimulation with anti-human CD3/CD28 Dynabeads and human IL-2 (for 24 h; T lymphocytes), F(ab)′2 anti-human IgG/IgM[38] and human IL-4 (for 24 h; B lymphocytes), human IL-2 (for 48 h; natural killer cells) or lipopolysaccharide (for 6 h; monocytes)[37].

The ATAC-seq data from the pancreatic islets of five donors without glucose intolerance and five EndoCβH1 cell line replicates, under resting conditions and after stimulation with IFN-γ and IL-1β for 48 h, were downloaded from the GEO (accession number GSE123404)[35].

The ATAC-seq data from cardiac fibroblasts (two fetal and three adult) were downloaded from the European Nucleotide Archive (https://www.ebi.ac.uk/ena/data/view/SRX2843570 and https://www.ebi.ac.uk/ena/data/view/SRX2843571) as a control cell type that we did not expect to be involved in the etiology of T1D[40].

Epigenome annotation tracks: We obtained chromHMM[100] tracks from diverse primary human cells from the NIH Epigenome Roadmap, http://dcc.blueprint-epigenome.eu/#/md/secondary_analysis/Segmentation_of_ChIP-Seq_data_20140811, and additional immune-specific human primary and cell lines from the Blueprint consortium, https://egg2.wustl.edu/roadmap/data/byFileType/chromhmmSegmentations/ChmmModels/coreMarks/jointModel/final.

Whole-blood eQTL summary statistics: Summary statistics from whole-blood *cis*-eQTL analysis from 31,683 individuals[42] were downloaded from https://eqtlgen.org.

Additional databases used in the priority-index drug target prioritization analysis were obtained through the relational database provided in the R package Pi (http://pi.well.ox.ac.uk:3010/download).

Code availability

Code used to generate the results presented in this paper is available at https://github.com/ccrobertson/t1d-immunochip-2020. The pipelines for processing ATAC-seq data are available at https://github.com/dfloresDIL/MEGA and http://pepatac.databio.org.

References

64. Manichaikul, A. et al. Robust relationship inference in genome-wide association studies. *Bioinformatics* **26**, 2867–2873 (2010).
65. Price, A. L. et al. Long-range LD can confound genome scans in admixed populations. *Am. J. Hum. Genet.* **83**, 127–147 (2008).
66. Chang, C. C. et al. Second-generation PLINK: rising to the challenge of larger and richer datasets. *Gigascience* **4**, 7 (2015).
67. Marchini, J. & Howie, B. Genotype imputation for genome-wide association studies. *Nat. Rev. Genet.* **11**, 499–511 (2010).
68. Willer, C. J., Li, Y. & Abecasis, G. R. METAL: fast and efficient meta-analysis of genomewide association scans. *Bioinformatics* **26**, 2190–2191 (2010).
69. Spielman, R. S., McGinnis, R. E. & Ewens, W. J. Transmission test for linkage disequilibrium: the insulin gene region and insulin-dependent diabetes mellitus (IDDM). *Am. J. Hum. Genet.* **52**, 506–516 (1993).
70. Taub, M. A., Schwender, H., Beaty, T. H., Louis, T. A. & Ruczinski, I. Incorporating genotype uncertainties into the genotypic TDT for main effects and gene-environment interactions. *Genet. Epidemiol.* **36**, 225–234 (2012).
71. Kazeem, G. R. & Farrall, M. Integrating case-control and TDT studies. *Ann. Hum. Genet.* **69**, 329–335 (2005).
72. Bottolo, L. & Richardson, S. Evolutionary stochastic search for Bayesian model exploration. *Bayesian Anal.* **5**, 583–618 (2010).
73. Benner, C. et al. Prospects of fine-mapping trait-associated genomic regions by using summary statistics from genome-wide association studies. *Am. J. Hum. Genet.* **101**, 539–551 (2017).
74. Excoffier, L. & Slatkin, M. Maximum-likelihood estimation of molecular haplotype frequencies in a diploid population. *Mol. Biol. Evol.* **12**, 921–927 (1995).
75. Wang, K., Li, M. & Hakonarson, H. ANNOVAR: functional annotation of genetic variants from high-throughput sequencing data. *Nucleic Acids Res.* **38**, e164 (2010).
76. Burren, O. S. et al. Chromosome contacts in activated T cells identify autoimmune disease candidate genes. *Genome Biol.* **18**, 165 (2017).
77. Corces, M. R. et al. An improved ATAC-seq protocol reduces background and enables interrogation of frozen tissues. *Nat. Methods* **14**, 959–962 (2017).
78. Harrow, J. et al. GENCODE: the reference human genome annotation for the ENCODE Project. *Genome Res.* **22**, 1760–1774 (2012).
79. Li, H. Minimap2: pairwise alignment for nucleotide sequences. *Bioinformatics* **34**, 3094–3100 (2018).
80. Gaspar, J. M. Improved peak-calling with MACS2. Preprint at *bioRxiv* https://doi.org/10.1101/496521 (2018).
81. Li, Q., Brown, J. B., Huang, H. & Bickel, P. J. Measuring reproducibility of high-throughput experiments. *Ann. Appl. Stat.* **5**, 1752–1779 (2011).
82. Liao, Y., Smyth, G. K. & Shi, W. FeatureCounts: an efficient general purpose program for assigning sequence reads to genomic features. *Bioinformatics* **30**, 923–930 (2014).
83. Trynka, G. et al. Disentangling the effects of colocalizing genomic annotations to functionally prioritize non-coding variants within complex-trait loci. *Am. J. Hum. Genet.* **97**, 139–152 (2015).
84. Smith, J. P. et al. PEPATAC: an optimized ATAC-seq pipeline with serial alignments. Preprint at *bioRxiv* https://doi.org/10.1101/2020.10.21.347054 (2020).
85. Jiang, H., Lei, R., Ding, S. & Zhu, S. Skewer: a fast and accurate adapter trimmer for next-generation sequencing paired-end reads. *BMC Bioinform.* **15**, 182 (2014).
86. Langmead, B. & Salzberg, S. L. Fast gapped-read alignment with Bowtie 2. *Nat. Methods* **9**, 357–359 (2012).
87. Neph, S. et al. BEDOPS: high-performance genomic feature operations. *Bioinformatics* **28**, 1919–1920 (2012).
88. Robinson, M. D., Mccarthy, D. J. & Smyth, G. K. edgeR: a Bioconductor package for differential expression analysis of digital gene expression data. *Bioinformatics* **26**, 139–140 (2010).
89. Robinson, M. D. & Oshlack, A. A scaling normalization method for differential expression analysis of RNA-seq data. *Genome Biol.* **11**, R25 (2010).
90. Fort, A. et al. MBV: a method to solve sample mislabeling and detect technical bias in large combined genotype and sequencing assay datasets. *Bioinformatics* **33**, 1895–1897 (2017).
91. Shabalin, A. A. Matrix eQTL: ultra fast eQTL analysis via large matrix operations. *Bioinformatics* **28**, 1353–1358 (2012).
92. Liu, B., Gloudemans, M. J., Rao, A. S., Ingelsson, E. & Montgomery, S. B. Abundant associations with gene expression complicate GWAS follow-up. *Nat. Genet.* **51**, 768–769 (2019).
93. Fairfax, B. P. et al. Innate immune activity conditions the effect of regulatory variants upon monocyte gene expression. *Science* **343**, 1246949 (2014).
94. Fairfax, B. P. et al. Genetics of gene expression in primary immune cells identifies cell type-specific master regulators and roles of HLA alleles. *Nat. Genet.* **44**, 502–510 (2012).

95. Andiappan, A. K. et al. Genome-wide analysis of the genetic regulation of gene expression in human neutrophils. *Nat. Commun.* **6**, 7971 (2015).
96. Kasela, S. et al. Pathogenic implications for autoimmune mechanisms derived by comparative eQTL analysis of $CD4^+$ versus $CD8^+$ T cells. *PLoS Genet.* **13**, e1006643 (2017).
97. Westra, H. et al. Systematic identification of trans eQTLs as putative drivers of known disease associations. *Nat. Genet.* **45**, 1238–1243 (2013).
98. Szklarczyk, D. et al. The STRING database in 2017: quality-controlled protein–protein association networks, made broadly accessible. *Nucleic Acids Res.* **45**, D362–D368 (2017).
99. R Core Team. *R: A Language and Environment for Computing*, https://www.R-project.org/ (R Foundation for Statistical Computing, 2020).
100. Ernst, J. & Kellis, M. Chromatin-state discovery and genome annotation with ChromHMM. *Nat. Protoc.* **12**, 2478–2492 (2017).

Acknowledgements

We thank the investigators and their studies for contributing samples and/or data to the current work, and the participants in those studies who made this research possible. These studies include the T1DGC, British 1958 Birth Cohort, Genetic Resource Investigating Diabetes (GRID), Consortium for the Longitudinal Evaluation of African-Americans with Early Rheumatoid Arthritis (CLEAR), Epidemiology of Diabetes Interventions and Complications (EDIC), Genetics of Kidneys and Diabetes Study (GoKinD), New York Cancer Project (NYCP), SEARCH for Diabetes in Youth study (SEARCH), Type 1 Diabetes TrialNet study (TrialNet), Tyypin 1 Diabetekseen Sairastuneita Perheenjäsenineen (IDDMGEN), Tyypin 1 Diabeteksen Genetiikka (T1DGEN), Northern Ireland GRID Collection, Northern Ireland Young Hearts Project, Hvidoere Study Group on Childhood Diabetes (HSG) and International HapMap Project. Additional institutions contributing samples are: British Diabetes Association (BDA), NIHR Cambridge BioResource, UK Blood Service (UKBS), Benaroya Research Institute (BRI), National Institute of Mental Health (NIMH), University of Alabama at Birmingham (UAB), University of Colorado, University of California San Francisco (UCSF), Medical College of Wisconsin (MCW) and Steno Diabetes Center. Samples and data from the T1DGC, EDIC and GoKinD can be obtained from the National Institute of Diabetes and Digestive and Kidney Diseases (NIDDK) Central Repository. This research utilizes resources provided by the T1DGC, a collaborative clinical study sponsored by the NIDDK, National Institute of Allergy and Infectious Diseases (NIAID), National Human Genome Research Institute (NHGRI), National Institute of Child Health and Human Development (NICHD) and Juvenile Diabetes Research Foundation (JDRF) and is supported by grant no. U01 DK062418 to S.S.R. The generation of chromatin-accessibility data on T1DGC samples was supported by grants from the NIDDK (grant nos DP3 DK111906 to S.S.R. and R01 DK115694 to P.C.). Further support was provided by the NIAID (grant no. P01 AI042288 to M.A.A.). The JDRF/Wellcome Diabetes and Inflammation Laboratory was supported by grants from the JDRF (grant no. 4-SRA-2017-473-A-A) and the Wellcome Trust (grant no. 107212/A/15/Z). Computation used the Oxford Biomedical Research Computing (BMRC) facility, a joint development between the Wellcome Centre for Human Genetics and the Big Data Institute supported by Health Data Research UK and the NIHR Oxford Biomedical Research Centre. Financial support was provided by a Wellcome Core Award (grant no. 203141/Z/16/Z). The views expressed are those of the author(s) and not necessarily those of the NHS, NIHR or Department of Health. While working on this project, C.C.R. was supported by a training grant from the US National Library of Medicine (grant no. T32 LM012416) and the Wagner Fellowship from the UVA. This work made use of data and samples generated by the 1958 Birth Cohort (NCDS), which is managed by the Centre for Longitudinal Studies at the UCL Institute of Education, funded by the Economic and Social Research Council (grant no. ES/M001660/1). Access to these resources was enabled via the MRC and Wellcome: 58FORWARDS grant no. 108439/Z/15/Z (The 1958 Birth Cohort: Fostering new Opportunities for Research via Wider Access to Reliable Data and Samples). Before 2015, biomedical resources were maintained under the Wellcome and Medical Research Council 58READIE Project (grant nos WT095219MA and G1001799). We acknowledge use of DNA samples from the NIHR Cambridge BioResource. We thank volunteers for their support and participation in the Cambridge BioResource and members of the Cambridge BioResource Scientific Advisory Board and Management Committee for their support of our study. We thank the NIHR Cambridge Biomedical Research Centre for funding. Access to Cambridge BioResource volunteers and their data and samples are governed by the Cambridge BioResource Scientific Advisory Board. Documents describing access arrangements and contact details are available at http://www.cambridgebioresource.org.uk/. The ethics for GRID were processed by the NRES Committee East of England Cambridge South MREC 00/5/44. We thank the following CLEAR investigators who performed recruiting: D. Conn (Grady Hospital and Emory University), B. Jonas and L. Callahan (University of North Carolina at Chapel Hill), E. Smith (Medical University of South Carolina), R. Brasington (Washington University) and L. W. Moreland (University of Pittsburgh). The CLEAR Registry and Repository was funded by the NIH Office of the Director (grant nos N01-AR-0-2247 (30 September 2000–29 September 2006) and N01-AR-6-2278 (30 September 2006–31 March 2012); S.L.B. Jr, principal investigator). Bio-samples and/or data for this publication were obtained from NIMH Repository and Genomics Resource, a centralized national biorepository for genetic studies of psychiatric disorders. The SEARCH for Diabetes in Youth Study (www.searchfordiabetes.org) is indebted to the many youth and their families, as well as their healthcare providers, whose participation made this study possible. SEARCH for Diabetes in Youth is funded by the Centers for Disease Control and Prevention (PA numbers 00097, DP-05-069 and DP-10-001) and supported by the NIDDK. The SEARCH site contract numbers are: Kaiser Permanente Southern California, U48/CCU919219, U01 DP000246 and U18DP002714; University of Colorado Denver, U48/CCU819241-3, U01 DP000247 and U18DP000247-06A1; Children's Hospital Medical Center (Cincinnati), U48/CCU519239, U01 DP000248 and 1U18DP002709; University of North Carolina at Chapel Hill, U48/CCU419249, U01 DP000254 and U18DP002708; University of Washington School of Medicine, U58/CCU019235-4, U01 DP000244 and U18DP002710-01; and Wake Forest University School of Medicine, U48/CCU919219, U01 DP000250 and 200-2010-35171. We acknowledge the support of the TrialNet group (https://www.trialnet.org), which identified study participants and provided samples and follow-up data for this study. The TrialNet group is a clinical trials network funded by the NIH through the NIDDK, NIAID and The Eunice Kennedy Shriver National Institute of Child Health and Human Development—through the cooperative agreements U01 DK061010, U01 DK061016, U01 DK061034, U01 DK061036, U01 DK061040, U01 DK061041, U01 DK061042, U01 DK061055, U01 DK061058, U01 DK084565, U01 DK085453, U01 DK085461, U01 DK085463, U01 DK085466, U01 DK085499, U01 DK085505 and U01 DK085509—and the JDRF. The contents of this article are solely the responsibility of the authors and do not necessarily represent the official views of the NIH or JDRF. Further support was provided by grants from the NIDDK (grant nos U01 DK103282 and U01 DK127404 to C.J.G.). DNA samples from the UAB were recruited, in part, with the support of grant nos P01-AR49084, UL1-TR001417 and UL1-TR003096 (to R.P.K.). We acknowledge the involvement of the Barbara Davis Center for Diabetes at the University of Colorado, supported by the following grants from the NIH NIDDK to M.J.R.: DRC P30 DK116073 and R01 DK032493. The collection of DNA samples at UCSF was supported by grant funding from the National Multiple Sclerosis Society (grant no. SI-2001-35701 to J.R.O.). Whole-genome-sequencing data production and variant calling was funded by an NHGRI Center for Common Disease Genomics award to Washington University in St. Louis (grant no. UM1 HG008853). This study used the TOPMed program imputation panel (version TOPMed-r2) supported by the NHLBI (www.nhlbiwgs.org). The TOPMed study investigators contributed data to the reference panel, which can be accessed through the Michigan Imputation Server (https://imputationserver.sph.umich.edu). The panel was constructed and implemented by the TOPMed Informatics Research Center at the University of Michigan (3R01HL-117626-02S1; contract HHSN268201800002I). The TOPMed Data Coordinating Center (3R01HL-120393-02S1; contract HHSN268201800001I) provided additional data management, sample identity checks and overall program coordination and support. We thank the studies and participants who provided biological samples and data for TOPMed. The individual members of the T1DGC and the SEARCH for Diabetes in Youth Study are listed in the Supplementary Note.

Author contributions

This study was conceptually designed by P.C., J.A.T. and S.S.R. The study was implemented by S.O.-G., P.C., J.A.T. and S.S.R. DNA samples for genotyping were managed by S.O.-G and E.F. L.S.W. contributed to data interpretation. D.J.M.C. provided statistical advice. Frozen T1DGC peripheral blood mononuclear cell samples for chromatin-accessibility profiling (ATAC-seq) were managed by P.C. and S.O.-G. ATAC-seq data generation at the UVA was led by S.O.-G. The generation of ATAC-seq data at the University of Oxford was led by A.J.C. Genotype data processing, quality control, imputation and statistical analyses were performed by W.-M.C., S.O.-G., J.R.J.I. and C.C.R. The chromatin-accessibility data processing and analysis was performed by A.J.C., D.F.S.C., J.R.J.I. and C.C.R. The EMSAs were performed by H.Y., with supervision from S.O.-G. D.B.D. provided samples for genotyping through the GRID. P.D. provided ImmunoChip genotyping data through the UKBS. J.H.B. provided samples for genotyping and data from the BRI. S.L.B. Jr provided samples for genotyping through the CLEAR consortium. P.K.G. provided samples for genotyping through the NYCP project. J.D., D.D., J.M.L., S.M. and A.S.S. provided samples for genotyping and data through the SEARCH for Diabetes in Youth study (SEARCH). C.J.G. and M.A.A. provided samples for genotyping through TrialNet. R.P.K., J.C.E., M.J.R., A.K.S., J.R.O. and F.P. provided samples for genotyping through their affiliated institutions and research programs. The manuscript was written by J.R.J.I. (under supervision by J.A.T.) and C.C.R. (under supervision by S.S.R.). All authors reviewed and approved the manuscript.

Competing interests

The authors declare no competing interests.

Additional information

Extended data is available for this paper at https://doi.org/10.1038/s41588-021-00880-5.

Supplementary information The online version contains supplementary material available at https://doi.org/10.1038/s41588-021-00880-5.

Correspondence and requests for materials should be addressed to J.A.T.

Peer review information *Nature Genetics* thanks the anonymous reviewers for their contribution to the peer review of this work. Peer reviewer reports are available.

Reprints and permissions information is available at www.nature.com/reprints.

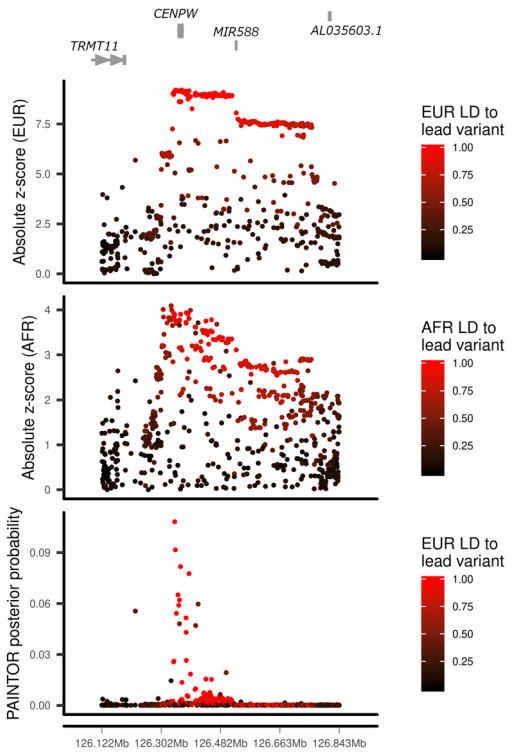

Extended Data Fig. 1 | Fine mapping of the chromosome 6q22.32 region. European (EUR, top panel) and African (AFR, middle panel) ancestry group association *z*-score statistics and posterior probabilities (bottom panel) from multi-ethnic fine mapping of EUR and AFR using PAINTOR. *z*-scores are colored by linkage disequilibrium (LD) to the lead PAINTOR-prioritized variant.

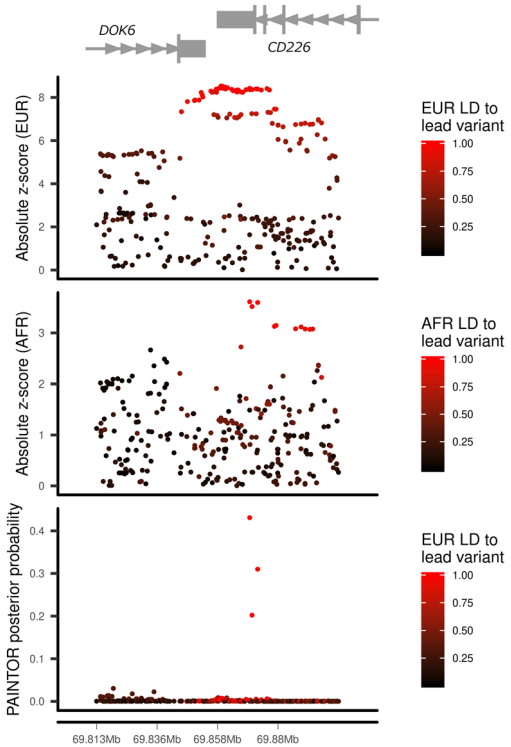

Extended Data Fig. 2 | Fine mapping of the chromosome 18q22.2 region. European (EUR, top panel) and African (AFR, middle panel) ancestry group association *z*-score statistics and posterior probabilities (bottom panel) from multi-ethnic fine mapping of EUR and AFR using PAINTOR. *z*-scores are colored by linkage disequilibrium (LD) to the lead PAINTOR-prioritized variant.

nature research

Corresponding author(s): John Todd (jatodd@well.ox.ac.uk)

Last updated by author(s): May 2, 2021

Reporting Summary

Nature Research wishes to improve the reproducibility of the work that we publish. This form provides structure for consistency and transparency in reporting. For further information on Nature Research policies, see our Editorial Policies and the Editorial Policy Checklist.

Statistics

For all statistical analyses, confirm that the following items are present in the figure legend, table legend, main text, or Methods section.

n/a	Confirmed
☐	☒ The exact sample size (*n*) for each experimental group/condition, given as a discrete number and unit of measurement
☐	☒ A statement on whether measurements were taken from distinct samples or whether the same sample was measured repeatedly
☐	☒ The statistical test(s) used AND whether they are one- or two-sided *Only common tests should be described solely by name; describe more complex techniques in the Methods section.*
☐	☒ A description of all covariates tested
☐	☒ A description of any assumptions or corrections, such as tests of normality and adjustment for multiple comparisons
☐	☒ A full description of the statistical parameters including central tendency (e.g. means) or other basic estimates (e.g. regression coefficient) AND variation (e.g. standard deviation) or associated estimates of uncertainty (e.g. confidence intervals)
☐	☒ For null hypothesis testing, the test statistic (e.g. *F*, *t*, *r*) with confidence intervals, effect sizes, degrees of freedom and *P* value noted *Give P values as exact values whenever suitable.*
☐	☒ For Bayesian analysis, information on the choice of priors and Markov chain Monte Carlo settings
☒	☐ For hierarchical and complex designs, identification of the appropriate level for tests and full reporting of outcomes
☐	☒ Estimates of effect sizes (e.g. Cohen's *d*, Pearson's *r*), indicating how they were calculated

Our web collection on statistics for biologists contains articles on many of the points above.

Software and code

Policy information about availability of computer code

Data collection	Illumina ImmuoChip genotype clusters were generated using the Illumina GeneTrain2 algorithm
Data analysis	Complete documentation of all code and tools used for all analyses can be found at https://github.com/ccrobertson/t1d-immunochip-2020 Below are software tools used for key steps in the analyses: Relationship inference and genotype QC - PLINK1.9 and KING (version 2.1.3) Genotype imputation – Michigan Imputation Server: phasing with Eagle (version 2.4) and imputation with Minimac4 Variant annotation – ANNOVAR (version released on Mon, 16 Apr 2018) Defining fine-mapping regions – R package "humarray" Case-control association analysis - SNPTEST (version 2.5.4) Family-based association analysis - PLINK1.9 Meta-analysis of association results – METAL (version released on 2011-03-25) Fine-mapping of associated regions - GUESSFM and PAINTOR Haplotype analyses of fine-mapped regions – GUESSFM, R package "mice", and custom code available in github repository ATAC-seq data processing – PEPATAC, minimap2 (version 2.17), bowtie2 (version 2.3.5), Picard tools (version 2.20.2), deeptools (version 3.3.0), macs2 (version 2.1.2), featureCounts (version 1.6.4), Skewer (version 0.2.2), bedops (version 2.4.35), R package "bigWig" Chromatin accessibility enrichment analyses - custom code available in github repository, GoShifter, DESeq2 Chromatin accessibility QTL analysis – QTLtools, R packages 'limma', 'edgeR' , 'MatrixEQTL', and 'meta' QTL colocalisation - R packages 'coloc' and 'locuscomparer' Drug target prioritisation - R package 'Pi' Data visualization - R packages 'ggplot2','cowplot', 'ggbio', 'GenomicRanges', 'gridExtra', 'RColorBrewer', and 'rtracklayer'

For manuscripts utilizing custom algorithms or software that are central to the research but not yet described in published literature, software must be made available to editors and reviewers. We strongly encourage code deposition in a community repository (e.g. GitHub). See the Nature Research guidelines for submitting code & software for further information.

Data

Policy information about availability of data

All manuscripts must include a data availability statement. This statement should provide the following information, where applicable:

- Accession codes, unique identifiers, or web links for publicly available datasets
- A list of figures that have associated raw data
- A description of any restrictions on data availability

All univariable summary statistics for genotype association with T1D (including imputed variants) are available through the NHGRI-EBI GWAS Catalog (GCST90013445 and GCST90013446). Chromatin accessibility QTL summary statistics are available through the Type 1 Diabetes Knowledge Portal.
Publicly available ATAC-seq - Raw FASTQ files were obtained from Gene Expression Omnibus (GEO) accession number GSE118189. These data included four individuals and 25 immune cell types under resting conditions and after stimulation with anti-human CD3/CD28 dynabeads and human IL-2 (for 24 hours, T lymphocytes), F(ab)'2 anti-human IgG/IgM 35 and human IL-4 (for 24 hours, B lymphocytes), human IL-2 (for 48 hours, NK cells), or LPS (for 6 hours, monocytes)34. ATAC-seq data from pancreatic islets of five donors without glucose intolerance and five EndoCβH1 cell line replicates, under resting conditions and after stimulation with IFN-γ and IL-1β for 48 hours were downloaded from GEO, accession number GSE123404 32.
ATAC-seq data from cardiac fibroblasts (two fetal and three adult) were downloaded from the European Nucleotide Archive (https://www.ebi.ac.uk/ena/data/view/SRX2843570 and https://www.ebi.ac.uk/ena/data/view/SRX2843571), as a control cell type that we did not expect to be involved in the aetiology of T1D 37.
Epigenome annotation tracks - chromHMM 76 tracks from diverse primary human cells were obtained from the NIH Epigenome Roadmap, http://dcc.blueprint-epigenome.eu/#/md/secondary_analysis/Segmentation_of_ChIP-Seq_data_20140811
and additional immune-specific human primary and cell lines from the Blueprint consortium, https://egg2.wustl.edu/roadmap/data/byFileType/chromhmmSegmentations/ChmmModels/coreMarks/jointModel/final.
Whole blood eQTL summary statistics - Summary statistics from whole blood cis eQTL analysis from 31,683 individuals39 were downloaded from https://eqtlgen.org.
Additional databases used in the Priority Index (Pi) drug target prioritization analysis were obtained through the relational database provided in the R package 'Pi' (http://pi.well.ox.ac.uk:3010/download).

Field-specific reporting

Please select the one below that is the best fit for your research. If you are not sure, read the appropriate sections before making your selection.

☒ Life sciences ☐ Behavioural & social sciences ☐ Ecological, evolutionary & environmental sciences

For a reference copy of the document with all sections, see nature.com/documents/nr-reporting-summary-flat.pdf

Life sciences study design

All studies must disclose on these points even when the disclosure is negative.

Sample size	No sample-size calculations were performed. Samples were collected according to resource availability. This represents the largest study of T1D to date. Genetic studies of this samples size have been shown to be well-powered to detect disease-associated genetic regions.
Data exclusions	Data were excluded according to the following quality control metrics (described in the Online Methods), which are in accordance with standards in the field for quality filtering of genetic data: Genetic data, variant filtering: (1) re-annotated ImmunoChip variant positions by aligning probe sequences to hg37 and removed any variants with less than a 100% match or multiple matches at different positions in the genome; (2) removed variants with call rates less than 98%; (3) removed variants with any discordance between duplicate or monozygotic twin samples, as confirmed by genotype-inferred relationships; (4) removed variants with Mendelian inconsistencies in more than 1% of informative trios or parent-offspring pairs, based on genotypeinferred relationships. Genetic data, sample filtering: We used X chromosome heterozygosity and Y chromosome missingness to identify and exclude participants with apparent sex chromosome anomalies or resolve inconsistencies with reported sex. Additionally, pedigree-defined and genotype-inferred sample relationships were compared and samples were excluded when inconsistencies could not be resolved. Relationships between families, within and across cohorts, were also checked. For each pair of related families observed, we randomly selected one to remove from association analysis. After resolving sex and relationship issues, samples with genotype call rate less than 98% were removed and variants with genotype frequencies deviating from Hardy-Weinberg Equilibrium ($p < 5\times10\text{-}5$) in unrelated European controls were excluded. ATAC-seq sample filtering: Libraries with transcription start site (TSS) enrichment scores less than 6 or fewer than 10 million aligned reads were excluded from analyses.
Replication	This study does not include a dedicated replication cohort. We made efforts to confirm the validity of our findings by comparing genetic associations with previously reported associations (with T1D and other diseases), as well as, by confirming concordance between results from subsets of the data, including multiple case-control cohorts of different ancestries and an affected trio cohort.

Randomization

There was no randomization involved in this study. Data were observational in nature, thus there was no opportunity for randomizing a treatment. Specifically, the treatment of interest is genetic variation and the outcome of interest is type 1 diabetes status. Neither can be randomized.

Blinding

There was no blinding involved in this study. Data were observational in nature, thus blinding is irrelevant to this study.

Reporting for specific materials, systems and methods

We require information from authors about some types of materials, experimental systems and methods used in many studies. Here, indicate whether each material, system or method listed is relevant to your study. If you are not sure if a list item applies to your research, read the appropriate section before selecting a response.

Materials & experimental systems

n/a	Involved in the study
☐	☒ Antibodies
☐	☒ Eukaryotic cell lines
☒	☐ Palaeontology and archaeology
☒	☐ Animals and other organisms
☒	☐ Human research participants
☒	☐ Clinical data
☒	☐ Dual use research of concern

Methods

n/a	Involved in the study
☒	☐ ChIP-seq
☒	☐ Flow cytometry
☒	☐ MRI-based neuroimaging

Antibodies

Antibodies used

ETS-1 Rabbit mAb
supplier: Cell Signaling Technology
catalog number: #14069
clone number: D8O8A
lot number: #2

Stat1 Rabbit mAb
supplier: Cell Signaling Technology
catalog number: #14994
clone number: D1K9Y
lot number: #5

Normal Rabbit IgG
supplier: Cell Signaling Technology
catalog number: #2729
clone number: polyclonal
lot number: #9

goat anti-human IgM/IgG/IgA antibody
supplier name: Jackson Immunoresearch
catalog number: 109-006-064
clone name: Polyclonal - RRID: AB_2337548
Final concentration: 10 ug/ml

MEGACD40L protein (recombinant human)
supplier name: ENZO lifesciences
catalog number: ALX-522-110-C010
clone name: NA
Final concentration: 0.15 ug/ml

recombinant human IL-21
supplier name: Peprotech
catalog number: 200-21
clone name: NA
Final concentration: 20 ng/ml

recombinant human IL-4
supplier name: Peprotech
catalog number: 200-04
clone name: NA
Final concentration: 20ng/ml

Validation

ETS-1 Rabbit mAb: Quality tested by immunoprecipitation and western blotting according to vendor's website (including images). The

Validation

vendor has also indicated that the antibody has been also validated by using SimpleChIP® Enzymatic Chromatin IP Kits.
STAT1 Rabbit mAb: Quality tested by immunoprecipitation and western blotting according to vendor's website. The vendor has also indicated that the antibody has been also validated by using SimpleChIP® Enzymatic Chromatin IP Kits.

Normal Rabbit IgG: Quality tested by immunoprecipitation and western blotting according to vendor's website (including images).

MMEGACD40L effect on immune cell activation was validated using the following protocol, according to the manufacturer (quantitative results provided): PBMCs (peripheral blood mononuclear cells) were incubated at 37°C, 5% CO2 for 48 hours in 48 well plates (1 x 106 cells per well) containing 200µl serum free test media with serially diluted MEGACD40L® (Prod. No. ALX-522-110), CD40L (Prod. No. ALX-522-015), or CD40L + 2µg/ml Enhancer (Prod. No. ALX-804-034). After treatment the cells were washed 3X with PBS + 1% BSA. The cells were dual stained for 2 hours at 4°C with mouse anti-human CD19 (PE conjugate) and mouse anti-human CD86 (APC conjugate). The cells were washed 2X with PBS + 1% BSA, then re-suspended In PBS. Samples were analyzed on a BD Facs Calibur flow cytometer. The data is presented as the percent of CD86 positive cells per CD19 positive B cells at each concentration.

Biological activity of the recombinant human IL-21 was determined by its ability to stimulate the proliferation of human ANBL-6 cells. According to manufacturer, the expected ED50 is ≤ 0.5 ng/ml, corresponding to a specific activity of ≥ 2 x106 units/mg.

Biological activity of the recombinant human IL-4 was determined by the dose-dependent stimulation of human TF-1 cells and the ED50 is ≤ 0.2 ng/ml, corresponding to a specific activity of ≥ 5 x 106 units/mg, according to manufacturer.

Eukaryotic cell lines

Policy information about cell lines

Cell line source(s)	Jurkat T cells were purchased from ATCC: Clone E6-1 (ATCC TIB-152)
Authentication	ATCC authenticates each distribution lot of cell lines. In addition, morphology of the cell line was checked by microscope, cells grew at a stable proliferation ratio, T cell receptor activation protocols confirmed IL-2 secretion
Mycoplasma contamination	Jurkat cells purchased from ATCC were not tested for mycoplasma.
Commonly misidentified lines (See ICLAC register)	The cell line used in this study is not listed in the ICLAC database of commonly misidentified lines.